

A Comparative Theoretical Study of the Hydrogen, Methyl, and Ethyl Chemisorption on the Pt(111) Surface

Garegin Papoian, Jens K. Nørskov, and Roald Hoffmann*

Contribution from the Department of Chemistry and Materials Science Center, Cornell University, Ithaca, New York 14853-1301, and Center for Atomic-scale Materials Physics, Department of Physics, Technical University of Denmark, Building 307, DK-2800 Lyngby, Denmark

Received September 27, 1999

Abstract: Chemisorbed hydrogen and various intermediate hydrocarbon fragments play an important role in the important reaction of ethylene hydrogenation to ethane, which is catalyzed by Pt(111). As a first step toward building a theoretical mechanism of the ethylene hydrogenation process, binding site preferences and geometries of chemisorbed hydrogen, methyl, and ethyl on the Pt(111) surface are presented and rationalized. State-of-the-art Pseudopotential Plane-wave Density Functional Theory is employed for calculating accurate binding energies and geometries for the adsorbates. A comprehensive theory of hydrogen and methyl chemisorption on Pt(111) is developed with the help of Crystal Orbital Hamilton Population formalism within the extended Hückel molecular orbital theory. The symmetry properties of the surface Pt orbitals as well as the mixing of Pt s, p, and d orbitals in pure Pt is shown to be crucial in determining the strength of subsequent interaction with an adsorbate. It is suggested that hydrogen moves freely on the Pt(111) surface while the methyl and ethyl groups are essentially pinned on the atop position. Strong agostic interactions between C–H bonds and surface Pt are proposed for methyl and ethyl on higher symmetry sites. The different nature of chemisorption on Pt and Ni surfaces is speculated. Theoretical results presented in this paper are generally consistent with the available experimental data.

1. Introduction

The hydrogenation of ethylene to ethane is one of the most fundamental and industrially important reactions in chemistry. To accelerate this reaction the Pt(111) surface is often used as a catalyst. The mechanistic aspects of this seemingly simple chemical process, a typical example of heterogeneous catalysis, are still incompletely understood. In an important development, Somorjai and co-workers have characterized with a Sum Frequency Generation (SFG) technique a number of intermediate hydrocarbon species under constant flow of gaseous reactants, but structural information on these is still lacking.¹ For instance, the combination of chemisorbed C₂H₅ and H, with consequent ethane desorption, was reasonably suggested to be the last, and perhaps the most important step of the ethylene hydrogenation process.^{1,2} However, as we will see in the discussion below, preferred binding sites, geometries, and binding energies of chemisorbed hydrogen and ethyl on Pt(111) are not well understood.

As a first step toward developing a theoretical understanding of the whole catalytic process, geometries, binding energies, and binding site preferences for intermediate chemisorbed hydrocarbon species and hydrogen have to be found and rationalized. In this paper, the first in a series, we build up a description of the chemisorption process for H, C₂H₅, and CH₃. The last fragment is not implicated in the ethylene hydrogenation mechanism; nevertheless, we use it as a simpler workhorse example since CH₃ adsorption is expected to be very similar to that of C₂H₅. In our theoretical treatment we model the surface

as an **abc** stacking of truly two-dimensional Pt(111) layers, thus taking fully into account the important metallic nature of the Pt(111) surface. To the best of our knowledge, we report in this paper the first state-of-the-art Plane-wave DFT studies on the ethyl and methyl chemisorption on the Pt(111) surface as well as the most elaborate treatment of chemisorbed hydrogen.

Given the lack of direct experimental structural evidence for a number of chemisorbed intermediate species on Pt(111), their geometries had to be determined otherwise. Pseudopotential Plane Wave Density Functional Theory³ appears to be an effective method for this purpose. Atomic coordinate optimizations and potential energy surface calculations are achieved with reasonable accuracy with this technique. Our calculations suggest that preferred binding modes for various hydrocarbons follow a very simple and intuitive pattern. To rationalize the latter we use the more transparent yet approximate extended Hückel molecular orbital theory.^{4–6}

We also analyze in detail the molecular orbital picture of H and CH₃ binding on the Pt(111) surface with the help of the recently developed Crystal Orbital Hamilton Population (COHP) method.^{7,8} The latter is a total energy partitioning scheme that allows one to compare the energetic contributions of various bonds to each other, a feature lacking in a more widely used Crystal Orbital Overlap Population (COOP) description (which is a total number of electrons partitioning scheme). The

(1) Cremer, P. S.; Su, X.; Shen, Y. R.; Somorjai, G. A. *J. Am. Chem. Soc.* **1996**, *118*, 2942.

(2) Zaera, F. *Surf. Sci.* **1989**, *219*, 453.

(3) Payne, M. C.; Teter, M. P.; Allan, D. C.; Arias, T. A.; Joannopoulos, J. D. *Rev. Mod. Phys.* **1992**, *64*, 1045.

(4) Hoffmann, R. *J. Chem. Phys.* **1963**, *39*, 1397.

(5) Hoffmann, R. *J. Chem. Phys.* **1964**, *40*, 2745.

(6) Hoffmann, R. *J. Chem. Phys.* **1964**, *40*, 2474.

(7) Dronskowski, R.; Blöchl, P. E. *J. Chem. Phys.* **1993**, *97*, 8617.

(8) Glassey, W. V.; Papoian, G. A.; Hoffmann, R. *J. Chem. Phys.* **1999**, *111*, 893.

Table 1. Extended Hückel Parameters

atom	orbital	H_{ii} (eV)	ζ_1	c_1	ζ_2	c_2	ref
Pt	6s	-9.077	2.554				67
	6p	-5.475	2.554				
	5d	-12.59	6.013	0.6334	2.696	0.5513	
C	2s	-21.4	1.625				4
	2p	-11.4	1.625				
H	1s	-13.6	1.3				4

investigation of a binding site preference for a given adsorbate is particularly amenable to a COHP analysis, since it allows one to attribute directly the total energy change among various adsorption sites to changes in a few bond (off-site) Hamilton Population values (see the Computational Details section for more information).

Our ultimate goal is to create a comprehensive “library” of small hydrocarbon adsorbates on the Pt(111) surface and rationalize their binding patterns. This, in turn, will help us understand the reaction pathways and activation energies for ethylene hydrogenation on the Pt(111) surface.

2. Computational Details

DFT. All calculations were carried out on a three-layer Pt(111) slab, with the Pt–Pt bond length of 2.83 Å. The latter distance is not the experimental Pt–Pt distance for bulk Pt (2.78 Å), but is the DFT optimized distance. There exists a certain advantage to using the theoretical distance: since the bulk Pt structure is at the minimum of the potential energy surface, unphysical calculated forces on the Pt atoms (which might occur if displacements are studied from a real bulk structure geometry) are avoided.

A 2×2 unit cell was used for describing the surface. We are aware that in hydrocarbon reactions the adsorption energies, as well as the adsorbate geometries, are in general coverage-dependent. We intend to address this problem in future studies. However, at this time it is not computationally feasible to carry out calculations for many adsorbate coverages; we have chosen the quarter-monolayer coverage as being representative of surface catalytic processes.

The length of the vacuum layer between two successive slabs is 9.24 Å. The electronic structure optimizations were carried out as described by Kresse and Furthmüller⁹ with the help of Dacapo 1.31, a program developed by Nørskov and co-workers. The Chadi-Cohen 18 k-point set was used to sample the Brillouin zone.¹⁰ Ultrasoft Vanderbilt pseudopotentials were employed to describe Pt, C, and H.¹¹ The Perdew-Wang91 GGA exchange-correlation functional was used for the electronic structure calculations.¹² The planewave expansion was shown to converge at 25 Ry. For better convergence of the numerical procedures, an electronic temperature of $kT = 0.10$ eV was assumed for the Fermi distribution. A dipole correction scheme was used to compensate for the surface dipole moment. Given the rigid nature of the Pt(111) surface, only the adsorbate atoms were allowed to relax, i.e., a fixed surface layer approximation was employed. The sum of all forces were converged below 0.05 eV/Å. Test calculations for chemisorbed H on a five-layer Pt(111) slab reproduced exactly the same H coordinates and essentially the same absolute binding energies (0.02 eV maximum deviation) compared with the three-layer slab. Thus, the latter serves as an excellent model for the Pt(111) surface.

Extended Hückel. All calculations were performed with “Yet Another extended Hückel Molecular Orbital Package (YAeHMOP)”, a program developed in our group.¹³ The optimized coordinates of various adsorbates on the Pt(111) surface were taken from the Planewave DFT calculations. A 54 k-point Chadi-Cohen scheme was

used to sample the Brillouin zone. The standard atomic parameters for Pt, C, and H are listed in Table 1 with the corresponding references.

COHP Formalism. Hamilton population partitioning of the total energy is a promising new tool in molecular orbital theory, which enables one to localize the total energy change to the immediate vicinity of the perturbation.^{7,8} For instance, when a methyl group is shifted from an atop position to a bridge site, the Hamilton populations of Pt–C, Pt–Pt, Pt–H, and C–H bonds are altered, helping to trace the exact origins for the binding site preference. For a molecule, the on- and off-site Hamilton populations are defined as follows:

$$HP_{\mu\mu} = \sum_i n_i |c_{\mu i}|^2 H_{\mu\mu} \quad (1)$$

$$HP_{\mu\nu} = \sum_i n_i \{c_{\mu i}^* c_{\nu i} H_{\mu\nu} + c_{\nu i} c_{\mu i}^* H_{\nu\mu}\} \quad (2)$$

where n_i is the population of MO i , $c_{\mu i}$ is the μ -th atomic orbital coefficient of MO i , and $H_{\mu\mu}$ and $H_{\mu\nu}$ are the diagonal and off-diagonal Hamiltonian matrix elements. Given the definitions above, the total energy of the system (in a one-electron formalism such as the extended Hückel method) may be written as:

$$E_{\text{tot}} = \sum_{\mu} HP_{\mu\mu} + \frac{1}{2} \sum_{\mu} \sum_{\nu \neq \mu} HP_{\mu\nu} \quad (3)$$

It is possible to further group Hamilton population terms into on-atom and off-atom contributions, which also sum up to the total energy as in eq 3.⁸ Another partitioning (now into fragments, groups of atoms) leads to on-fragment and off-fragment Hamilton populations. Thus, chemical intuition about natural functional groups may be quantified and examined with the help of the COHP analysis.⁸ We have recently described in detail the extended analogue of eq 3; a simple chemical picture may still be found behind the cumbersome mathematics.⁸

Since the COHP analysis is carried out on the energy scale, negative energies (COHP contributions) indicate bonding interactions and positive energies (COHP contributions) indicate antibonding interactions. The COHP curves shown later in the paper will appear flipped around the vertical axis if compared with the more familiar COOP curves (crystal orbital overlap population), which are bonding in the positive region and antibonding in the negative region. We have shown previously that Hamilton populations are simply energy-weighted overlap populations, which explains the obvious similarity of COHP and COOP curves (except for the sign).⁸

In earlier studies in this group, it was suggested that the total binding energy for a given chemisorbed hydrocarbon be partitioned into ionic and covalent parts.¹⁴ The former represents the gain in energy as an electron is transferred, prior to adsorption, from a higher-lying Fermi state in the metal to the lower-lying half-filled hydrocarbon orbitals (for example, the sp^3 orbital in the CH_3 radical). The ionic energy, although providing for most of the apparent binding energy, is obviously insensitive to the binding site preference. Having this in mind, we have chosen to fragment the composite slab-adsorbate system as Pt_{12}^+ and H^- or CH_3^- . In the following discussion, when we refer to COHP values for a pure Pt slab or an isolated adsorbate, we mean the correspondingly charged species. This charge partitioning has no effect on the COHP analysis for the composite adsorbate–Pt slab system.

We want to make clear the underlying philosophy of our analysis. We trust the DFT-calculated energetics much more than we do those calculated with the very approximate eH method. However, it is difficult to analyze the DFT results with respect to origins, while for the eH method we have a tested analytical tool, the COHP. The latter analysis may be constructed for the DFT method as well; however, in this case the total energy is no longer a simple sum of individual COHP terms, rendering difficult a straightforward comparison between adsorbates having different geometries. So we will follow a 2-fold process: we will check that the energetics we trust (DFT) is followed by the eH

(9) Kresse, G.; Furthmüller, J. *Comput. Mater. Sci.* **1996**, *6*, 15.

(10) Chadi, D. J.; Cohen, M. L. *Phys. Rev. B* **1973**, *8*, 5747.

(11) Laasonen, K.; Pasquarello, A.; Car, R.; Lee, C.; Vanderbilt, D. *Phys. Rev. B* **1993**, *47*, 10142.

(12) Perdew, J. P.; Chevary, J. A.; Vosko, S. H.; Jackson, K. A.; Pederson, M. R.; Singh, D. J.; Fiolhais, C. *Phys. Rev. B* **1992**, *46*, 6671.

(13) Landrum, G. A.; Glassey, W. V.: <http://overlap.chem.cornell.edu:8080/yaehmop.html>, 1999.

(14) Zheng, C.; Apeloig, Y.; Hoffmann, R. *J. Am. Chem. Soc.* **1988**, *110*, 749.

method (this will turn out to be so) and then we will proceed with our analysis within the COHP/eH formalism.

3. Results and Discussion

In the earlier works of Somorjai and co-workers¹⁵ and Hoffmann and co-workers¹⁴ a model was suggested for binding of the simplest hydrocarbons on the (111) surfaces of transition metals. Stated simply, the model claims that upon hydrocarbon fragment binding to a surface, carbons tend to complete their tetravalency. For example, the methyl group would bind strongest to the atop position, methylene to the bridge positions, and methylidyne to the triply bridging (fcc or hcp) positions. Recent DFT calculations of small hydrocarbons on a Pt₈ molecule are also consistent with the tetravalency principle.¹⁶

One sees the limitation of the tetravalency rule when the adsorption of H on the Pt(111) surface is considered. Although H is not a hydrocarbon, its binding patterns are expected to be similar to those of the methyl group (i.e. strong preference for the atop site). However, Somorjai and co-workers suggested that for overlap reasons hydrogen should be bound more strongly to the bridge site.¹⁵ But it turns out from our calculations that neither atop H nor bridging H are more stable: in fact theory indicates that hydrogen has a very flat potential energy surface on Pt(111). Given the absence of definite experimental structural data even for the simplest chemisorbed alkanes, the tetravalency principle remains rather speculative.¹⁷ To make matters worse, it has been strongly suggested (both experimentally and theoretically) that the methyl group binds preferentially on the 3-fold site on Ni(111) and Cu(111), prompting one to question altogether the validity of the tetravalency rule.^{18–24} One would like to have an adsorption theory that would explain *simultaneously* site preferences of both H and hydrocarbons on the Pt(111) surface, as well as on Ni(111) and Cu(111).

If the relative stability of two binding sites is to be compared when tetravalency cannot be achieved at either site, then it is not clear how to choose the most stable position. For instance, the ease of diffusion for chemisorbed ethylidyne might carry important implications for the mechanism of ethylene hydrogenation at high pressures. However, one cannot predict beforehand whether the atop or the bridge position would be the transition state for the surface diffusion. The adsorption of unsaturated hydrocarbons such as ethylene and acetylene is also not covered directly by the tetravalency principle.

Given the lack of experimental structural determinations for the great majority of the adsorbed hydrocarbon species, we believe that one must reexamine (and modify if necessary) the original tetravalency principle using the two-dimensional surface treatment of the Planewave DFT theory, currently the most sophisticated theoretical method for studying surfaces. In the following discussion we first examine DFT binding energies and structural features of chemisorbed H, CH₃, and C₂H₅ on the Pt(111) surface and compare with the available experimental

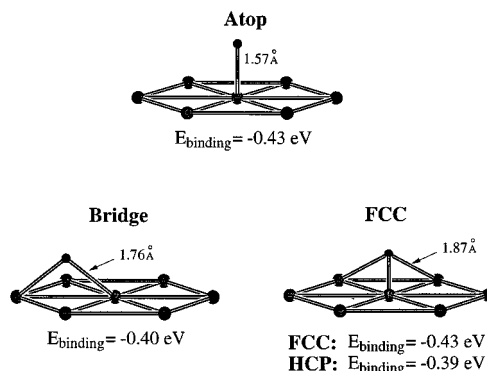
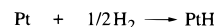


Figure 1. Three-layer Pt(111) slab covered by a 2×2 atomic hydrogen layer. Only seven surface Pt atoms are shown. Geometries and binding energies were optimized using the Planewave DFT.

data. Then, we apply the COHP formalism within the extended Hückel theory to build up a comprehensive orbital theory of H and CH₃ chemisorption on Pt(111). We demonstrate that the proper consideration of crystal orbital symmetries at different binding sites, along with the predictable patterns of adsorbate induced Pt s–d and p–d rehybridization, provides a consistent picture of H and CH₃ (C₂H₅) chemisorption on Pt(111). We also speculate on the origin of the difference of the nature of adsorbate bonding for Pt and Ni.

3.1. DFT Results: H on Pt(111). We have calculated the binding energies of hydrogen on various Pt surface sites as a difference between the total energy of a PtH slab and the sum of the energies of a pure Pt slab and molecular hydrogen. The symbol Pt in the scheme **1** stands for the Pt₁₂ stoichiometry in the unit cell. We keep to this notation throughout the following discussion, when we consider binding energy calculations for the CH₃ and C₂H₅ chemisorption. As may be inferred from **1**,



1

our calculated binding energies are given per one adsorbed H atom. One has to double these numbers to compare them with the experimental results which are usually provided per H₂ molecule (see the later discussion). In essence, our calculated binding energies represent the heats of adsorption for corresponding gaseous species.

The geometries and binding energies of H on atop, bridge, fcc, and hcp sites are given in Figure 1. The triply bridging fcc and hcp sites differ only by the presence or the absence of a Pt atom underneath the respective Pt₃ triangle. There are no significant differences between the adsorbate geometries on the fcc and hcp sites, so we choose to show the adsorbate on the fcc site only for all adsorbates (in the subsequent molecular orbital analysis we also discuss only the fcc site). From the geometrical point of view, hydrogen comes progressively closer (vertically) to the surface as it moves from the atop site to the bridge site and to the fcc/hcp sites.

The calculated binding energies for the various sites are found to be the same within the accuracy of the Planewave DFT method ($E_{\text{binding}} \approx -0.40$ eV). In addition, our calculated activation energies for hopping (diffusion) between various sites suggest a very flat potential energy surface. The activation energy for hopping between the atop and the other sites ranges from 0.09 to 0.13 eV, while the activation energy for the bridge-hcp diffusion is merely 0.02 eV. Thus, we expect at low enough coverage that H will be effectively smeared over the surface. A similar conclusion was previously reached for H on Ni(100)

(15) Minot, C.; van Hove, M. A.; Somorjai, G. A. *Surf. Sci.* **1982**, *127*, 441.

(16) Kua, J.; Goddard, W. A., III *J. Chem. Phys. B* **1998**, *102*, 9492.

(17) Zaera, F. *Chem. Rev.* **1995**, *95*, 2651.

(18) Yang, Q. Y.; Maynard, K. J.; Johnson, A. D.; Ceyer, S. T. *J. Chem. Phys.* **1995**, *102*, 7734.

(19) Lin, J.-L.; Bent, B. E. *Chem. Phys. Lett.* **1992**, *194*, 208.

(20) Leo, M. B.; Yang, Q. Y.; Seyer, S. T. *J. Chem. Phys.* **1987**, *87*, 2424.

(21) Bengaard, H. S.; Nørskov, J. K. To be submitted for publication.

(22) Kratzer, P.; Hammer, B.; Nørskov, J. K. *J. Chem. Phys.* **1996**, *105*, 5595.

(23) Burghgraef, H.; Jansen, A.; van Santen, R. *Chem. Phys.* **1993**, *177*, 407.

(24) L Whitten, J. *J. Phys. Chem.*, **1992**, *96*, 5529.

and Ni(111) by treating chemisorbed H motion quantum-mechanically.²⁵

Given the small size of the H atom compared with the surface Pt atoms, the difficulties in the experimental determination of the H binding sites on Pt(111), in the assignment of vibrational frequencies, and in the estimation of the heats of adsorption have produced a lively discussion in the literature in the last three decades.^{26–42} Christmann and co-workers, for instance, did not observe any ordering of H on Pt(111) up to a 0.8 monolayer H coverage in their Low-Energy Electron Diffraction (LEED) experiments.²⁶ An ordered H submonolayer on Pt(111) has not been observed in the subsequent studies as well. From our DFT calculations we have determined a very flat potential energy surface for low-coverage H on Pt(111). Thus, we expect H to move freely on the surface. This conclusion is not inconsistent with the absence of an experimentally observed ordered H submonolayer on Pt(111) (which do exist for other transition metals; for instance, the well-ordered quarter-monolayer 2×2 H superstructure on Ni(111)^{38,43}). The softness of the H in-plane vibrational modes, as determined from High-Resolution Electron Energy Loss Spectroscopy (HREELS) studies by Richter and Ho, also points in the same direction.³⁷

The heats of adsorption per H₂ dissociating on Pt(111) were determined from Thermal Desorption Spectroscopy (TDS) studies to lie in the range from 0.70 to 0.83 eV.^{27,38,41,42} Considering the uncertainties of experimental heats of adsorption for H on Pt(111), our calculated binding energies per H₂ molecule, found to be 0.8 eV, are in excellent agreement with the experimental data.

For a single monolayer H coverage on Pt(111), a 3-fold adsorption binding site was suggested for H, as evidenced by Electron Energy Loss Spectroscopy (EELS), HREELS, He diffraction, Low-Energy Recoil Scattering (LERS), and Neutron Scattering experiments.^{29,31–35,40} For both fcc and hcp H we have calculated a 1.87 Å Pt–H distance, which is in the 1.8–1.9 Å range estimated from the He diffraction and LERS studies.^{31–35} In an interesting development, Eberhardt and co-workers proposed that subsurface H is the most thermodynamically stable state at room temperature on the basis of their Angle-Resolved Photoemission Spectroscopy (ARPS) studies; however, this suggestion was refuted later by the He diffraction experiments of Lee, Cowin, and Wharton.^{30,31} Given the potential importance of this question for the hydrogenation mechanism, we have calculated binding energies for subsurface H in the

Table 2. Binding Energies (per H₂) for a Single Monolayer H on Pt(111)

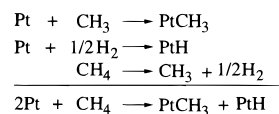
binding site	atop	bridge	HCP	FCC
binding energy	−0.77 eV	−0.71 eV	−0.75 eV	−0.85 eV

octahedral holes, which was suggested by Eberhardt and co-workers. We have found a strong destabilization of 0.88 eV per H for subsurface H as compared with surface H. Thus, we do not expect a spontaneous surface–subsurface transition, in agreement with Lee, Cowin, and Wharton.

The LERS experiments have indicated strongly that the 3-fold adsorption site is the fcc site.³⁵ Since for a quarter-monolayer coverage we expect H to be very mobile on the surface, the strong preference for the fcc site exhibited by a monolayer H motivated us to carry out calculations for that coverage as well. The results, presented in Table 2, do indeed suggest that the fcc site is favored by 0.1 eV per H₂, in agreement with the experimental results. Therefore, close H–H contacts in the monolayer H coverage alter somewhat the potential energy surface calculated for the quarter-monolayer coverage. A reviewer pointed out that one could have expected a more dramatic change in adsorption energies, as hydrogen atoms are in close proximity for the monolayer hydrogen coverage. To address this issue, we carried out additional COHP calculations which in turn indicated very small H–H interactions at a lattice spacing of 2.83 Å. Furthermore, this conclusion is in agreement with the saturation coverage $\theta = 2$ for H on the W(100) surface,⁴⁴ suggesting that hydrogen atoms are too small to overlap efficiently at transition metal lattice spacing separations.

Summing up, our Planewave DFT calculations strongly suggest a flat potential energy surface for a quarter-monolayer H on Pt(111), implying a high mobility of H on the surface. For the single monolayer coverage, the H–H interactions render the fcc site the most stable, in agreement with the experimental results. Our calculated binding energies and the Pt–H bond length agree well with the experimental data.

3.2. DFT: CH₃ and C₂H₅ on Pt(111). We examine next the geometries and binding energies of chemisorbed CH₃ on Pt(111). Scheme 2 illustrates how the binding energy is



2

calculated. We make an assumption here that CH₄ dissociates on two separate Pt slabs into a PtCH₃ slab and a PtH slab. This binding energy should approximate the energy of CH₄ dissociation into CH₃ and H at low coverage on a single Pt surface. A possible alternative is to calculate the binding energy as the difference between the total energies of a PtCH₃ slab and the sum of total energies of a Pt slab and a CH₃ radical. We have decided that the CH₄ dissociation scheme below would be more appropriate from the broader perspective of the ethylene hydrogenation process (in which the desorption of ethane from C₂H₅ and H is thought to be the last step). We emphasize that for a given adsorbate only the energy difference between various binding sites matters, i.e., any binding energy calculation scheme should reproduce the same differences.

We find that the methyl group is bound strongest on the atop site, weaker on the bridge site, and weakest on the fcc/hcp sites. A small negative binding energy is found for atop CH₃,

(25) Puska, M. J.; Nieninen, R. M.; Manninen, M.; Chakraborty, B.; Holloway, S.; Nørskov, J. K. *Phys. Rev. Lett.* **1983**, *51*, 1081.

(26) Christmann, K.; Ertl, G.; Pignet, T. *Surf. Sci.* **1976**, *54*, 365.

(27) Newuwenhuys, B. E. *Surf. Sci.* **1976**, *59*, 430.

(28) Demuth, J. E. *Surf. Sci.* **1977**, *65*, 369.

(29) Baró, A. M.; Ibach, H.; Bruchmann, H. D. *Surf. Sci.* **1979**, *88*, 384.

(30) Eberhardt, W.; Greuter, F.; Plummer, E. W. *Phys. Rev. Lett.* **1981**, *46*, 1085.

(31) Lee, J.; Cowin, J. P.; Wharton, L. *Surf. Sci.* **1983**, *130*, 1.

(32) Batra, I. P. *Surf. Sci.* **1984**, *137*, L97.

(33) Batra, I. P.; Barker, J. A.; Auerbach, D. J. *J. Vac. Sci. Technol. A* **1984**, *A2*, 943.

(34) Batra, I. P. *Surf. Sci.* **1984**, *148*, 1.

(35) Koelman, B. J. J.; de Zwart, S. T.; Boers, A. L.; Poelsema, B.; Verheij, L. K. *Phys. Rev. Lett.* **1986**, *56*, 1152.

(36) Poelsema, B.; Brown, L. S.; Lenz, K.; Verheij, L. K.; Comsa, G. *Surf. Sci.* **1986**, *171*, L395.

(37) Richter, L. J.; Ho, W. *Phys. Rev. B* **1987**, *36*, 9797.

(38) Christmann, K. *Surf. Sci. Rep.* **1988**, *9*, 1.

(39) Feibelman, P. J.; Hamann, D. R. *Surf. Sci.* **1987**, *182*, 411.

(40) Renouprez, A. J.; Jobic, H. *J. Catal.* **1988**, *113*, 509.

(41) Godbey, D. J.; Somorjai, G. A. *Surf. Sci.* **1988**, *204*, 301.

(42) Atli, A.; Alnot, M.; Ehrhardt, J. J.; Bertolini, J. C.; Abon, M. *Surf. Sci.* **1992**, *269/270*, 365.

(43) Heinz, K.; Hammer, L. Z. *Phys. Chem.* **1996**, *197*, 173.

(44) Alnot, P.; Cassuto, A.; King, D. A. *Surf. Sci.* **1989**, *215*, 29.

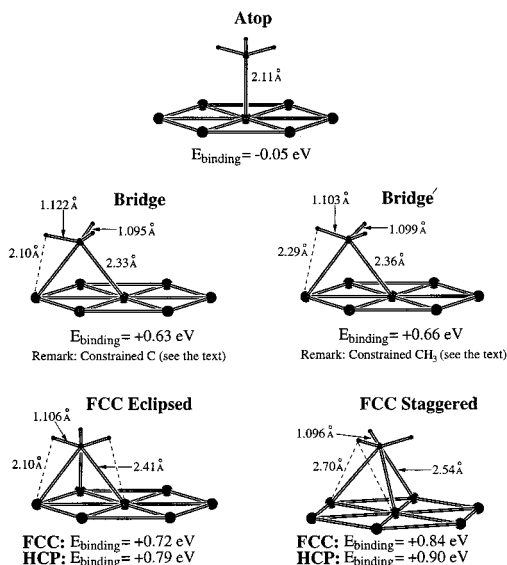


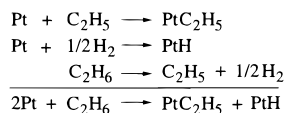
Figure 2. Three-layer Pt(111) slab covered by a 2×2 CH₃ layer. Only seven surface Pt atoms are shown. Geometries and binding energies were optimized using the Planewave DFT.

indicating a very weak exothermicity for the dissociative CH₄ chemisorption on the Pt(111) surface. When we attempted to optimize freely CH₃ in a bridging position, the methyl group drifted toward the more stable atop position. Consequently, we restricted in the first case the horizontal carbon coordinates above the midpoint of the Pt–Pt bond. In an alternative calculation, the coordinates of all atoms in the CH₃ fragment were first transferred from the atop to the bridge position. Then only vertical movements were allowed during the optimization. The energy difference between two optimizations is rather small, but in the former case a significant elongation of the C–H bond parallel to the Pt–Pt bond is observed. Furthermore, the CH₃ group is slightly tilted so to maximize the H–Pt interactions.

For a number of other chemisorbed hydrocarbons on Pt(111) we have noticed significant interactions between their hydrogen atoms and the Pt surface (to be reported later). As for the chemisorbed bridge CH₃ (carbon atom constrained horizontally on the bridge site), one observes in those cases a short Pt–H distance and a correspondingly weakened C–H bond. Thus, the CH₃ group is well prepared for the cleavage of the C–H bond on this site.

Similar short Pt–H close contacts are also found for CH₃ on fcc/hcp positions, as may be inferred from Figure 2. For these binding sites eclipsed CH₃ is 0.11 eV more stable than the staggered one which in turn is consistent with the stabilizing nature of Pt–H interactions (this difference is only 0.001 eV for on-top CH₃). The optimized Pt–H bond length of 2.10 Å is actually significantly shorter than the Pt–C bond length of 2.41 Å. This type of interaction is reminiscent of agostic interactions observed in organometallic compounds.⁴⁵ We elucidate the molecular orbital picture of these surface agostic interactions in the subsequent analysis.

The binding energies of chemisorbed C₂H₅ were calculated using the same approximation as for the CH₃ case: C₂H₆ was assumed to dissociate on two independent Pt slabs (see 3). If



3

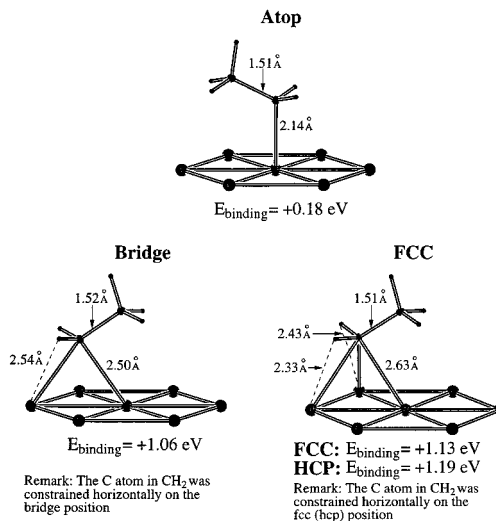


Figure 3. Three-layer Pt(111) slab covered by a 2×2 C₂H₅ layer. Only seven surface Pt atoms are shown. Geometries and binding energies were optimized using the Planewave DFT.

the surface coverage is low enough (i.e. adsorbates do not interact much with each other) one would expect this scheme to approximate reasonably well the C₂H₆ dissociation on a single Pt(111) surface.

As we have mentioned earlier, desorption of C₂H₆ from chemisorbed C₂H₅ and H is thought to be the last step of the ethylene hydrogenation mechanism. According to our calculated binding energies this last step is somewhat exothermic, i.e., 0.18 eV would be released if atop C₂H₅ would combine with surface H (see Figure 3). On the other hand, the dissociation of gas-phase ethane on Pt(111) is not expected to be a spontaneous process.

The binding site preferences and geometrical features of C₂H₅ and CH₃ are quite similar (compare Figures 2 and 3). The bridge, fcc, and hcp positions are greatly destabilized compared to the atop site. The calculations of Kua and Goddard on ethyl on a molecular Pt₈ model of the surface obtain energetic results qualitatively similar to ours, but do not provide a detailed analysis of the origins of the computed energetics.¹⁶ Furthermore, the C₂H₅ group in the former positions drifted toward the atop site during the full geometrical optimization. Therefore, the horizontal coordinates of the C bound to the surface were frozen at the bridge, fcc, and hcp positions correspondingly.

Significantly short agostic-type interactions between C–H bonds and the Pt surface persist for fcc/hcp ethyl positions as well (see Figure 3). In the bridge case the C–C bond was aligned parallel to the Pt–Pt bond; then the distance between methyl C and Pt was found to be 2.92 Å. The C–C bond length in chemisorbed C₂H₅ is ≈ 0.01 Å shorter than the C–C bond length calculated for isolated ethane (1.525 Å).

Unfortunately, we cannot compare directly our calculated structural features and binding energies with the experimental results, as the latter are lacking. However, Reflection Adsorption Infrared Spectroscopy (RAIRS) and HREELS determination of CH₃ vibrational frequencies point to a local C_{3v} symmetry site, which would correspond to both atop and 3-fold positions.^{46–49}

(45) Brookhart, M.; Green, M. L. H.; Wong, L.-L. *Prog. Inorg. Chem.* **1988**, 36, 1.

(46) Oakes, D. J.; Newell, H. E.; Rutten, F. J. M.; McCoustra, M. R. S.; Chesters, M. A. *J. Vac. Sci. Technol. A* **1996**, 14, 1439.

(47) Wenger, J. C.; McCoustra, M. R. S.; Chesters, M. A. *Surf. Sci.* **1996**, 360, 93.

(48) Fan, J.; Trenary, M. *Langmuir* **1994**, 10, 3649.

(49) Sheppard, N.; De La Cruz, C. *Adv. Catal.* **1998**, 42, 181.

It is generally thought that CH₃ is bound in the atop site, but there is no direct structural evidence supporting this.^{17,49} The vibrational analysis for a chemisorbed ethyl group suggests a local C_s symmetry, which does not rule out any adsorption site.^{46,50–52,49} The symmetrical C–H stretching modes were not softened for both CH₃ and C₂H₅, as opposed to the observation of the CH₃ C–H mode softening on Ni(111) and Cu(111).^{49,18–20} We argue later in the paper that CH₃ on a 3-fold site is expected to be engaged in strong agostic interactions with the surface Pt atoms, which in turn should soften C–H vibrations even more compared to Ni and Cu. We believe that the absence of this effect points to atop chemisorption for CH₃ and C₂H₅ on Pt(111), as opposed to the 3-fold sites on Cu(111) and Ni(111). From this perspective, “hard” CH₃ symmetrical C–H stretching vibrations observed on Ru(0001) also indicate an atop adsorption.⁴⁹

Given the extremely low sticking coefficients of methane and ethane adsorption on Pt(111), the corresponding heats of adsorption have not been determined experimentally. Nevertheless, one can estimate these as the difference of the activation energies for forward and backward reactions **2** and **3** (the hydrocarbons and hydrogen coexist on the same surface in this case). The activation energy for methane adsorption was suggested to be 0.76 eV based on quantum-dynamical modeling of CH₄ molecular beam experiments.^{53,54} The back reaction of methane formation from chemisorbed CH₃ and H was found to be activated by 0.74 eV from the TPD experiments.⁵⁵ Thus, we estimate the experimental heat of methane chemisorption on Pt(111) to be +0.02 eV, which essentially coincides with our calculated value of –0.05 eV, given the degree of uncertainty for both experimental and theoretical results.

By modeling the results of supersonic molecular beam experiments, McCoustra, Chesters, and co-workers proposed a 0.36 eV activation energy for ethane chemisorption on Pt(111).⁵⁶ As for the back reaction, ethyl hydrogenation to ethane, Zaera suggested that the activation energy is less than 0.26 eV, based on the TPD experiments.⁵⁷ Hence, we estimate the heat of ethane adsorption on Pt(111) to be more than +0.10 eV, which is consistent with the +0.18 eV value from our DFT calculations. Given the very challenging nature of many abovementioned experiments, one should not, perhaps, interpret too closely the numerical estimates of the activation energies. In addition, it should be noted here that positive thermodynamic bonding energies (as defined here, with respect to gaseous *molecules*) are not to be taken as an indicator that C₂H₅ (or CH₃) are not bound: in fact these are strongly bound species. For instance, chemisorbed CH₃ must be in proximity with chemisorbed H and a significant activation barrier must be overcome for CH₄ to desorb from the surface.

In summary, our Planewave DFT calculations indicate a flat potential energy surface for H, while CH₃ and C₂H₅ are preferentially bound on the atop site. Given the isolobal relationship of these three species, such diverging behavior remains to be explained. The nature of presumably agostic interactions between C–H bonds in CH₃ and C₂H₅ at certain

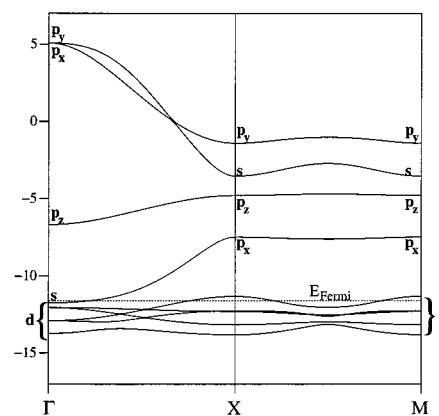


Figure 4. The band structure of a one-layer Pt(111) slab. Crystal orbitals at the high-symmetry sites originate from the indicated atomic orbitals.

binding sites and surface Pt atoms must be explained as well. In the remaining part of this paper we build up a detailed molecular orbital theory of the H and CH₃ chemisorption which addresses these and some other issues.

3.3. The Electronic Structure of a Pure Pt Slab. A necessary first step toward constructing a detailed theory of H and CH₃ chemisorption on Pt(111) is to understand the basic electronic features of a pure Pt slab. One way to accomplish this goal would be to analyze the band structure for bulk Pt and, then, to follow the changes when the bulk is cleaved (hypothetically) so to expose the (111) surface. However, we chose an alternative path: a single Pt(111) layer serves as our starting point. The band structure for such a layer calculated within the extended Hückel formalism is shown in Figure 4 (the Pt(111) layer is perpendicular to the *z* axis).

As one would expect, s,p and d orbitals behave in a very different manner. The latter are rather contracted, thus producing significantly narrow bands. On the other hand, the s,p block is very broad, spanning a 20 eV energy window. One may notice in Figure 4 that there is a clear separation of d and s,p bands, although certain mixing does occur. Only in the vicinity of Γ , a high symmetry point in the reciprocal space, does the s band dip below the Fermi level.

As two more layers are added to the original single Pt(111) layer, the band structure becomes more complicated; however, the basic features persist. Major changes occur with the p_z and d_{z²} bands which engage in the interlayer interactions. The COHP curves for the surface Pt d–d, s–d, and p–d interactions are presented in Figure 5 (notice that the energy window has changed from Figure 4). Using some simple concepts from the molecular orbital perturbation theory, one could rationalize the curves in Figure 5 in the following way.

The crystal orbitals of the pure Pt(111) slab may be derived from atomic orbitals by turning on consecutively intra-band and inter-band interactions (see Figure 6). First, only like orbitals are allowed to interact, thus broadening into separate d, s, and p bands. Because both s and p bands are wide and largely overlapping, for the sake of simplicity we have combined the s and p blocks in Figure 6 into a single s,p block. Although d and s,p blocks interpenetrate each other to a certain extent, they are drawn separately for clarity.

Coming back to the COHP curves in Figure 5 we notice that the narrow d block consists of a lower-lying d–d bonding part and the higher lying d–d antibonding part. As the interactions among orbitals of different kind are turned on in step II (Figure 6), a predictable pattern of mixing occurs. Specifically, higher-lying s and p bands mix into the lower-lying d bands in a

(50) Lloyd, K. G.; Roop, B.; Campion, A.; White, J. M. *Surf. Sci.* **1989**, *214*, 227.

(51) Hoffmann, H.; Gruffiths, P. R.; Zaera, F. *Surf. Sci.* **1992**, *262*, 141.

(52) Newell, H. E.; McCoustra, M. R. S.; Chesters, M. A.; De La Cruz, C. *J. Chem. Soc., Faraday Trans.* **1998**, *94*, 3695.

(53) Luntz, A. C.; Harris, J. *Surf. Sci.* **1991**, *258*, 397.

(54) Harris, J.; Simon, J.; Luntz, A. C.; Mullins, C. B.; Rettner, C. T. *Phys. Rev. Lett.* **1991**, *67*, 652.

(55) Zaera, F. *Surf. Sci.* **1992**, *262*, 335.

(56) Newell, H. E.; Oakes, D. J.; Rutten, F. J. M.; McCoustra, M. R. S.; Chesters, M. A. *Faraday Discuss.* **1996**, *105*, 193.

(57) Zaera, F. *J. Phys. Chem.* **1990**, *94*, 8350.

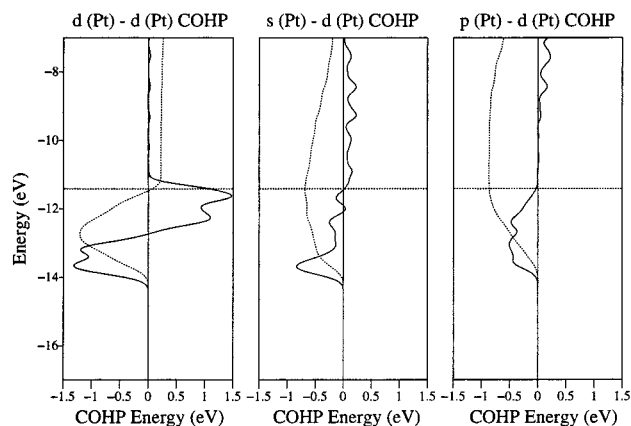


Figure 5. The COHP curves (solid lines) and their respective integrations (dotted lines) for d–d, s–d, and p–d interactions within the surface Pt layer in a three-layer model.

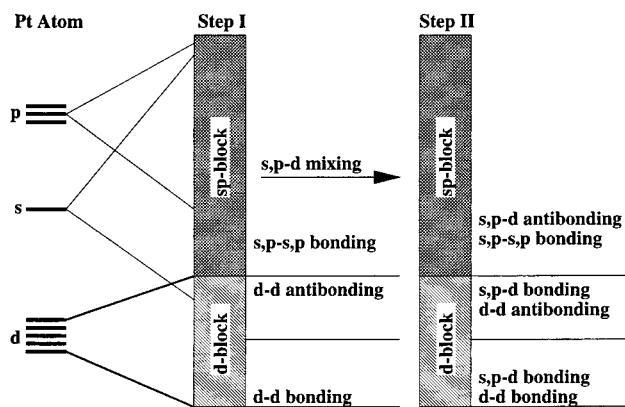


Figure 6. A hypothetical two-step construction of Pt–Pt bonding in bulk Pt. Step I: Like orbitals only are allowed to interact forming corresponding bands. Step II: High-energy bands mix into the low-energy ones in a bonding way, while the low-energy bands mix into the high-energy ones in an antibonding way.

bonding manner, while opposite mixing occurs in the reverse direction.⁵⁸ For instance, the s–d and p–d COHP curves are bonding in the d block region (Figure 5) while they are antibonding in the s,p block region.

The abovementioned interactions between d and s,p bands have far-reaching consequences for the subsequent adsorption of various species. We explore these as we go along; here we elaborate only on the effect of this mixing for adsorption in the atop site. Since we treat the surface as a two-dimensional extended system, there are many k-points in the corresponding reciprocal space which represent the crystal (surface) orbitals for the Pt slab. However, certain interactions may be rationalized from a local viewpoint, as illustrated for d and s,p mixing in Figure 7. The latter interactions have a profound effect on the shape of the resulting surface orbitals: only the “tall” orbitals at the top of the d block and the bottom of the s,p block are well prepared for a good overlap with an adsorbate orbital pointing toward the atop site.

The designations “tall” and “short” refer to s, d_{z^2} combinations whose form is more realistically indicated by the contour diagrams of representative surface orbitals at Γ for a one-layer Pt(111) model in Figure 8. The vertical hybridization of bonding MO 4 and antibonding MO 13 follow clearly the previously described patterns. And it is very important in determining the subsequent interactions with chemisorbed fragments.

(58) Albright, T.; Burdett, J.; Whangbo, M.-H. *Orbital Interactions in Chemistry*; John Wiley & Sons: New York, 1985.

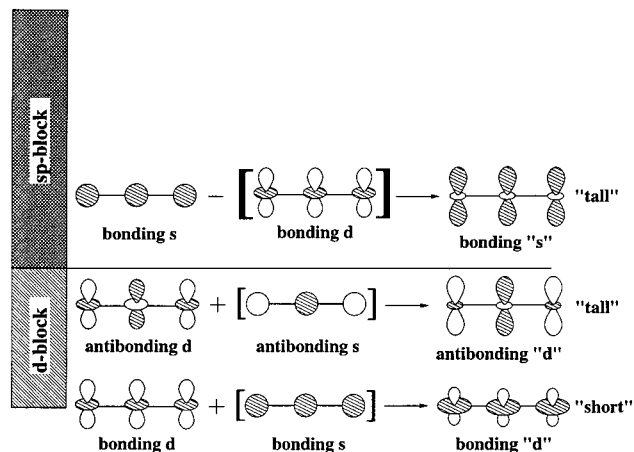


Figure 7. A schematic representation of s– d_{z^2} hybridization in the surface Pt layer shown in a side view (z perpendicular to the surface).

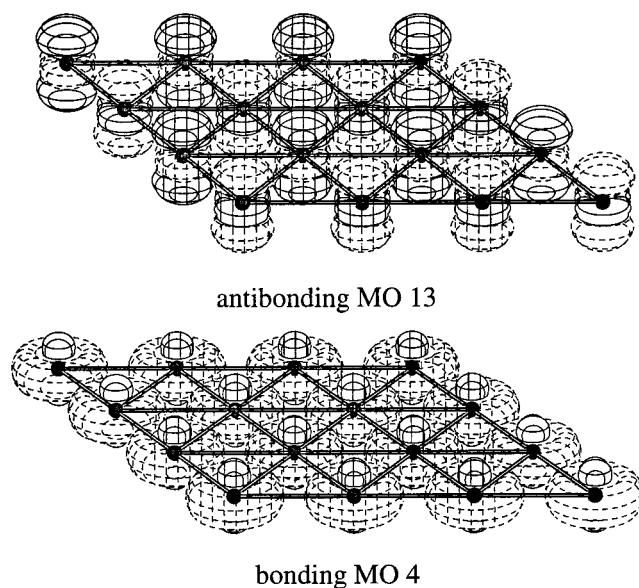


Figure 8. “Tall” and “short” orbitals: the d_{z^2} derived surface orbitals at Γ for a one-layer Pt(111) model.

Having outlined the basic features of the Pt slab electronic structure, we are ready to interact the surface with corresponding adsorbates. H is the simplest adsorbate that one can think of; we built a detailed molecular orbital theory for its chemisorption first.

3.4. H on the Atop Site. As we have suggested in the previous discussion, the top antibonding portion of the d block is well prepared for strong interactions with the H adsorbate. This is indeed what is observed: only that part of the d(Pt)–d(Pt) COHP curve gets pushed above the Fermi level and becomes partially depopulated (Figure 9). This in turn leads to stronger surface Pt–Pt bonds, a somewhat unusual conclusion since one expects that surface bonds get weakened upon chemisorption.⁵⁹ It happens that only Pt–Pt bonds are affected which originate from Pt underneath adsorbed H. We will come back to this point a little later.

To gain further insight into the nature of adsorbate–surface interactions, we have plotted in Figure 10 s(H)–s(Pt), s(H)–p(Pt), and s(H)–d(Pt) off-site COHP curves. The s(H)–d(Pt) interactions are easiest to interpret; they serve as the extended analogue of a two-orbital mixing mechanism: the bonding region near the H band at -1.5 eV is stabilized and the

(59) Silvestre, J.; Hoffmann, R. *J. Vac. Sci. Technol. A* **1986**, *4*, 1336.

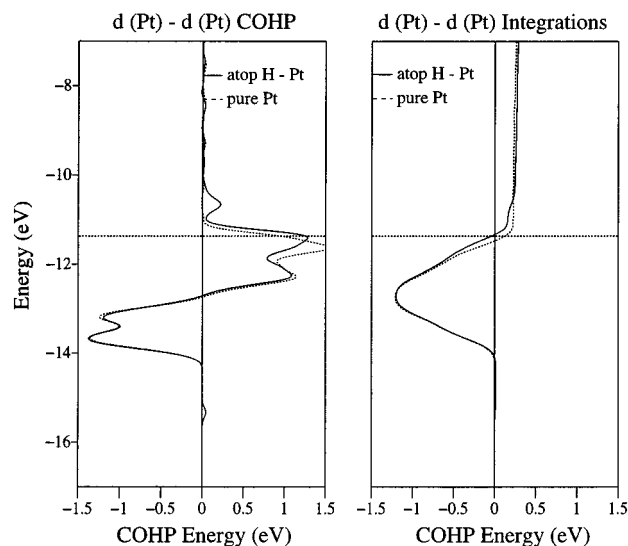


Figure 9. The superposition of COHP curves (left) and their respective integrations (right) for $d(\text{Pt})-d(\text{Pt})$ interactions for surface Pt–Pt bonds in atop chemisorbed H (solid lines) and a pure Pt slab (dotted lines). Only Pt–Pt bonds originating from Pt under H were considered.

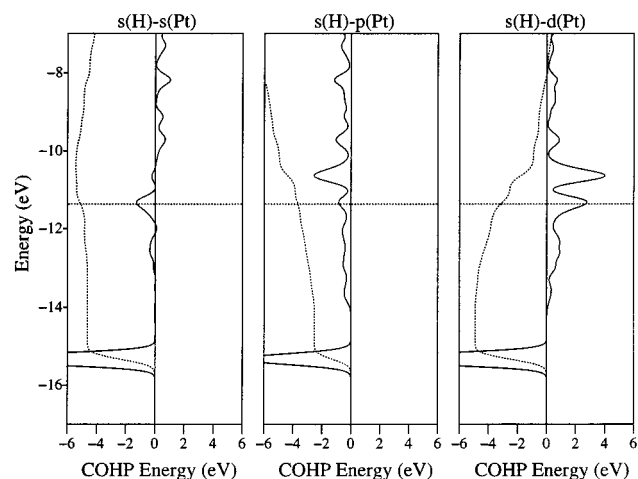


Figure 10. The COHP curves (solid lines) and their respective integrations (dotted lines) for $s(\text{H})-s(\text{Pt})$, $s(\text{H})-p(\text{Pt})$, and $s(\text{H})-d(\text{Pt})$ interactions for the atop bound H.

antibonding region ranging through the d block is destabilized. If the d block were completely filled initially, and no transfer of electrons to other bands were to occur, than the interaction of filled H band and filled d bands would be overall destabilizing, similar to a well-understood two-orbital four-electron repulsion of filled orbitals ($\text{He}\cdots\text{He}$, two lone pairs approaching). However, the d band in pure Pt is partially depopulated due to mixing with s,p bands; in addition, these Pt d bands (which are pushed above the Fermi level by interacting with H) dump their electrons into the Fermi sea. The antibonding $s(\text{H})-d(\text{Pt})$ states around the d block do not fully reverse the bonding character of the lower-lying states, thus an overall stabilization occurs (the corresponding Hamilton population integrates to -3.38 eV). A related analysis for other transition metals was previously carried out by Hammer and Nørskov.⁶⁰

On the contrary, the $s(\text{H})-s(\text{Pt})$ COHP is *bonding* throughout the d-band region, turning antibonding right above it (Figure 10). The $s(\text{H})-p(\text{Pt})$ COHP is bonding in the whole energy window shown in Figure 10, becoming antibonding only in states very high in energy. One may reconcile such diverging

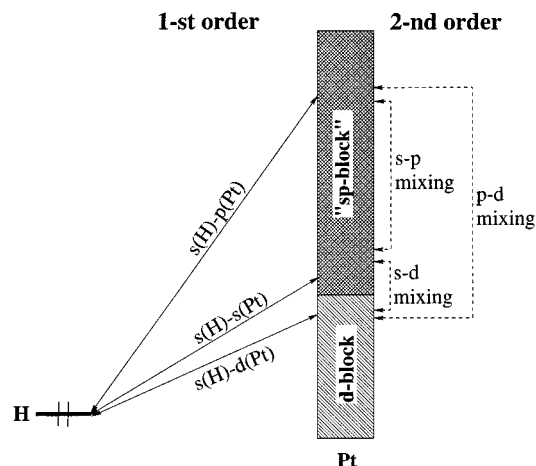


Figure 11. A schematic representation of the atop H and Pt slab interactions through perturbative first- and second-order mixing of H and Pt crystal orbitals.

behavior of Pt d, s, and p orbitals by considering the surface–H interactions as a two-step perturbation process (see Figure 11). In the first step, only the interactions between H and Pt crystal orbitals are turned on, without the latter mixing into each other. This produces a bonding COHP region near the H band and corresponding antibonding regions near the centers of gravity of corresponding Pt d, s, and p bands (the position of the H band is found below all Pt states). The center of gravity of the p band is out of the energy window of Figure 10, thus the $s(\text{H})-p(\text{Pt})$ antibonding states are very high in energy.

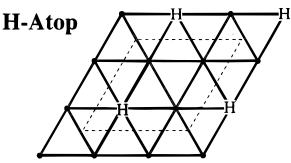
Second-order mixing of Pt crystal orbitals results in the more complicated COHP curve patterns observed for Pt s and p orbitals (Figure 10). The higher-lying s and p bands mix into the d-band region in a *bonding* way with respect to the Pt–H interactions. The higher-lying p bands mix into the s-band region also in a *bonding* way. The lower-lying d bands mix in an *antibonding* way into s- and p-band regions above. All these features are clearly seen in Figure 10.

We expect that our perturbational treatment of adsorbate–surface interactions provides a quite general qualitative description of adsorbate-induced mixing of surface crystal orbitals. Now we turn to the quantitative details of H–Pt interactions.

The important Hamilton population values for atop adsorbed H on Pt(111) are presented in Table 3. The contribution of numerous other Hamilton population terms is not shown, neither in Table 3 nor in subsequent tables. However, one must bear in mind that only the sum of all on-site and off-site COHP terms, the extended Hückel total energy, determines the relative stability for the given adsorption geometry compared with other alternatives. As far as the relative importance of $s(\text{H})-s(\text{Pt})$, $s(\text{H})-p(\text{Pt})$, and $s(\text{H})-d(\text{Pt})$ interactions is concerned, the latter is the weakest (-3.38 eV). Thus, the greatest share of Pt–H bond strength is contributed by the H s-orbital interaction with the Pt s and p orbitals. As may be deduced from Figure 10, the $s(\text{H})-s(\text{Pt})$ and $s(\text{H})-d(\text{Pt})$ COHP curves integrate to approximately the same values just above the H band; however, filled antibonding states in the d block render the d interactions less bonding. The $s(\text{H})-s(\text{Pt})$ COHP integration, on the contrary, increases monotonically up to the Fermi level, for the reasons outlined earlier.

Another remarkable feature found in Table 3 is the differentiation of the surface Pt–Pt bonds: those that originate from Pt directly underneath H become noticeably *stronger* (-2.06 vs -1.94 eV in a pure Pt slab). The Hamilton population values for the remaining surface Pt–Pt bonds, as well as “bulk”

(60) Hammer, B.; Nørskov, J. K. *Nature* **1995**, *376*, 238.

Table 3. COHP Decomposition of Various Interactions for an Atop Chemisorbed H on Pt(111)^a


H-Pt COHP Analysis

s(H)-s(Pt)	-4.99 eV
s(H)-p(Pt)	-3.62 eV
s(H)-d(Pt)	-3.38 eV

Pt-Pt off-site COHP (in eV)

H-Atop		Pure Pt slab	
Surface Pt-Pt	-2.06	Surface Pt-Pt	-1.94
"Bulk" Pt-Pt	-1.88	"Bulk" Pt-Pt	-1.94

Surface Pt orbital populations

	d	s	p
Pure Pt slab	9.35	0.42	0.20
H-Atop *	8.75	0.55	0.37

*Only Pt atoms connected to H are considered

^a Surface Pt-Pt bonds involving the Pt atoms connected with H are indicated with bold lines. The atomic orbital populations are presented as well.

Pt-Pt bonds (those within the bottom two Pt layers), decrease in absolute magnitude by approximately 0.05 eV. The two latter phenomena may be tied up together into a consistent picture by the following conjecture: the H pushes over the Fermi level selectively *only* those Pt-Pt states which are just underneath the Fermi level, thus depopulating them (compare in Table 3 the d-orbital population values for pure Pt and the composite H-Pt system). As evidenced by Figure 9, these depopulated states are d-d antibonding in character; therefore, the corresponding Pt-Pt bonds strengthen. The dumped electrons enter the states near the Fermi level, antibonding in character for the remaining Pt-Pt bonds, weakening these bonds to some small degree.

The comparison of d(Pt)-d(Pt) COHP curves for other surface Pt-Pt bonds with the ones in a pure Pt slab (similar to the comparison in Figure 9; not shown here) indicates that these are not really affected by the interaction of the surface with H. The Hamilton population values for these bonds are also consistent with them behaving differently than the Pt-Pt bonds underneath H. Thus, H produces a horizontal polarization of the Pt surface states. We finish the atop H discussion by exploring in more detail the molecular orbital mechanism behind this polarization.

To simplify the picture as much as we can, we only examine one layer of Pt(111) atoms interacting with H in the atop position. For a pure Pt(111) layer, consider first a primitive unit cell consisting of just one Pt atom (Figure 12). In the Brillouin zone of the corresponding reciprocal lattice, we pick a set of general (low-symmetry) k-points, labeled L₁-L₄ ($\mathbf{k} = (\pm 0.25, \pm 0.25)$), which are representative of the surface crystal orbitals. We are going to follow the evolution of the d_{z²} crystal orbitals at these k-points, as the Pt surface interacts with the incoming H.

However, one more step has to be taken before proceeding with the H adsorption. The desired 2×2 hydrogen coverage

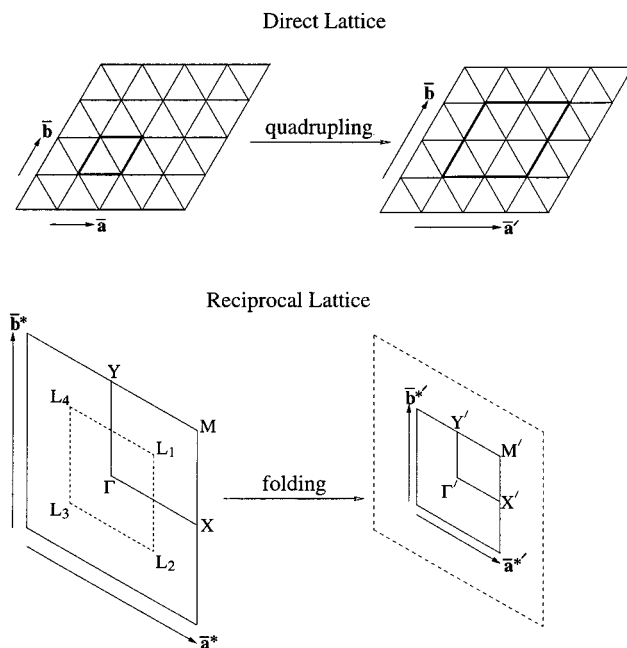


Figure 12. A unit cell quadrupling in the direct space leads to quadruple folding in the reciprocal space. The outer parts of the new Brillouin zone are translated by new reciprocal vectors $\bar{\mathbf{a}}^{*'}$ and $\bar{\mathbf{b}}^{*'}$ into the inner zone. Points L₁, L₂, L₃, L₄ ($\pm 0.25, \pm 0.25$) in the larger Brillouin zone become superimposed on top of each other at point M' (0.5, 0.5) in the new zone.

renders the original primitive unit cell improper from the translational symmetry point of view. The wave functions must be "prepared" for subsequent interaction with H by 2×2 quadrupling of the unit cell, which in turn results in the corresponding Brillouin zone being four times smaller (Figure 12). The parts of the larger original Brillouin zone which do not fit into the new cell are translated into it by the new lattice vectors of the reciprocal space ($\bar{\mathbf{a}}^{*'}$ and $\bar{\mathbf{b}}^{*'}$ in Figure 12). This process is often called "folding".

Following the procedure described above, the points L₁-L₄ get superimposed on top of each other at the new high-symmetry point M' (0.5, 0.5). Since the original wave functions at L₁-L₄ are described by fractional k coordinates ($\pm 0.25, \pm 0.25$), their Bloch sums contain both real and imaginary components. A simple linear combination of crystal orbitals related by time-reversal symmetry (i.e. L₁ and L₃; L₂ and L₄) leads to the real wave functions shown in Figure 13.

Two degenerate pairs of d_{z²} crystal orbitals (CO) emerge from the linearization described above (Figure 13). CO 7 and CO 8 consist of d_{z²} orbitals centered on Pt rows alternating with Pt rows having zero d_{z²} coefficients. The nearest-neighbor interactions between Pt's are bonding, therefore these crystal orbitals are found low in energy (-12.73 eV). The antibonding counterparts CO 19 and CO 20 are at higher energy (-12.03 eV), as expected. The important difference between these two sets of degenerate orbitals is highlighted by the way higher-lying s bands mix into them. As we have discussed earlier, the bonding d_{z²} bands are "short", and the antibonding ones are "tall" (see Figure 7). Thus, the antibonding set should interact much more strongly with H than bonding CO 7 and CO 8.

At this point we have not made a distinction between degenerate CO 19 and CO 20, since any linear combination of them would produce a valid new set of degenerate orbitals for a pure Pt layer. The interaction with H dramatically breaks this degeneracy: CO 20 has a node at the Pt's bonded to H while CO 19 interacts strongly. CO 19 depopulates by being pushed

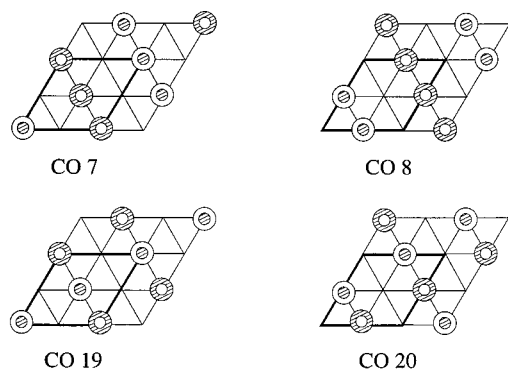


Figure 13. Four d_{z^2} crystal orbitals (CO) at M' for a one-layer Pt_4 surface. The twin circles here are icons for a d_{z^2} orbital seen from the top. These orbitals are derived from the original complex crystal orbitals at k -points L_1 , L_3 , and L_2 , L_4 by adding and subtracting the respective wave functions. The incoming H atoms are to interact with the Pt atoms at the corners of the highlighted unit cells.

above the Fermi level, which in turn strengthens surface Pt–Pt bonds originating from Pt underneath H. The remaining surface Pt–Pt bonds remain largely unaffected. Thus, a strong polarization of the surface bonding results. It should be mentioned here that a similar analysis may be carried out for other k -point sets, which represent alternative directions of d_{z^2} rows (Figure 13).

In summary, the nature of the s,d and p,d hybridization of the surface crystal orbitals in a pure Pt slab plays a very important role in determining which states are better suited for a subsequent interaction with the adsorbate. In the case of atop H, s bands mix into the high-lying antibonding portion of the d_{z^2} states in such a way as to make them “taller”, thus having a larger overlap with the H s orbital. These states partially depopulate due to the interaction with H, dumping their electrons into Pt–Pt antibonding states of the other Pt–Pt bonds. The Pt–Pt bonds near the chemisorption site are actually strengthened. The original degeneracy of the surface Pt–Pt bonds is broken by H-induced bond reorganization; a significant surface polarization results.

3.5. H on the Bridge and fcc Sites. When an H atom is moved from an atop to a bridge position, according to our Planewave DFT calculations the absolute value of its binding energy is slightly reduced by 0.03 eV (see Figure 1). Extended Hückel calculations (using DFT optimized H coordinates) point to the same trend, although somewhat exaggerated; the bridge site is destabilized by 0.18 eV. Given the respective accuracy range of both methods, we think it is fair to say that both atop and bridge sites are pretty much equally favored for the H adsorption. Since a great preference for atop adsorption would have been inferred from the direct application of the tetravalency (monovalency for H) principle, we wish to explore the reasons for this apparent discrepancy.

A COHP analysis of selected interactions for bridge-chemisorbed H is given in Table 4. A quick comparison with the atop case reveals a significant strengthening of the $s(H)$ – $s(Pt)$ Hamilton population, which is partially compensated by weakening of the $s(H)$ – $p(Pt)$ and $s(H)$ – $d(Pt)$ interactions. Overall, the H to two bridge Pt HP is -0.47 eV more favorable than the corresponding H to atop Pt HP. If non-nearest-neighbor interactions are included as well, the latter difference grows to -0.73 eV. As far as the H to surface Pt interactions are concerned, the bridge site is strongly favored for the H chemisorption. However, the total energy change points to the opposite conclusion, implying that other effects are at work.

A very important feature of the COHP formalism is the additivity of the on- and off-site Hamilton population terms to

Table 4. COHP Decomposition of Various Interactions for a Bridge-Chemisorbed H on $Pt(111)$ ^a

H-Pt COHP Analysis		
	H-Bridge	H-Atop
$s(H)$ – $s(Pt)$	-5.87 eV	-4.99 eV
$s(H)$ – $p(Pt)$	-3.39 eV	-3.62 eV
$s(H)$ – $d(Pt)$	-3.20 eV	-3.38 eV
Total H-Pt	-12.47 eV	-12.00 eV

Pt-Pt off-site COHP (in eV)			
	H-Bridge	Pure Pt slab	
Surface Pt-Pt	-1.12	Surface Pt-Pt	-1.94
	-1.88	Surface Pt-Pt	-1.94
"Bulk" Pt-Pt	-1.83	"Bulk" Pt-Pt	-1.88

Surface Pt orbital populations			
	d	s	p
Pure Pt slab	9.35	0.42	0.20
H-Bridge*	9.16	0.47	0.24
H-Atop*	8.75	0.55	0.37

*Only Pt atoms connected to H are considered

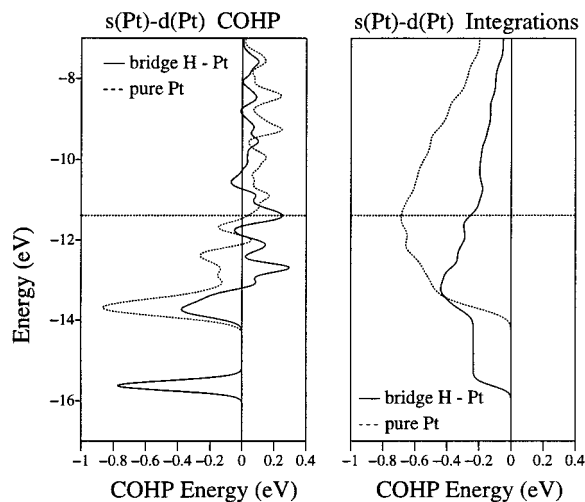
^a Surface Pt–Pt bonds directly underneath H are indicated with bold lines. The atomic orbital populations are presented as well.

the total energy of the system. Moreover, a destabilization in the total energy may be traced to the decrease of the absolute value of the sum of all off-site terms. For instance, the sum of all off-site terms for the bridge chemisorbed H is -121.78 eV, compared to -123.26 eV for the atop case. This difference exaggerates the change in the total energies ($+0.18$ eV in extended Hückel calculations) because the remaining on-site terms work in the opposite direction. Since the H–Pt Hamilton population is more favorable for the bridge site, it must be overcompensated by weakening of Pt–Pt bonds (these are the only remaining off-site HP elements).

This is indeed what happens. The Pt–Pt bond directly underneath the bridge H is significantly weakened to -1.12 eV, compared to -1.88 eV for other surface Pt–Pt bonds. Another interesting feature seen in Table 4 is the lesser depopulation of the d bands for bridge H compared with atop H. The weakening of Pt–Pt bonds (as opposed to strengthening observed for the atop H case), as well as the smaller degree of the d -block depopulation, provides a hint that there must be a qualitatively different molecular orbital picture behind H chemisorption on the bridge site.

To investigate this supposition we have carried out an orbital by orbital COHP decomposition of the Pt–Pt off-site Hamilton population (only for the bridge bond). A quick glance at Figure 14 reveals that the destabilizing s – d ($+0.43$ eV), p – d ($+0.26$ eV), and d – d ($+0.24$ eV) Hamilton populations are mainly responsible for the overall Pt–Pt bond weakening. The superposition of $s(Pt)$ – $d(Pt)$ COHP curves and their respective integrations for bridge chemisorbed H on $Pt(111)$ and pure $Pt(111)$ indicates that the strongly bonding s – d states in the d -block region for pure Pt become partially antibonding for the composite H–Pt system (Figure 14).

The main reason behind the gain of some antibonding character of the originally bonding s – d states in the d -block region is H-induced second-order mixing of empty higher-lying



Pt-Pt COHP

	H-bridge*	Pure Pt
s-s	-0.35 eV	-0.31 eV
s-p	-0.18 eV	-0.12 eV
s-d	-0.25 eV	-0.68 eV
p-p	-0.05 eV	-0.01 eV
p-d	-0.61 eV	-0.87 eV
d-d	+0.31 eV	+0.07 eV
Total	-1.12 eV	-1.93 eV

* Only Pt atoms connected to H are considered

Figure 14. The superposition of COHP curves (left graph) and their respective integrations (right graph) for s(Pt)-d(Pt) interactions for surface Pt-Pt bonds in bridge chemisorbed H (solid lines) and a pure Pt slab (dotted lines). Only the Pt-Pt bond directly underneath H was considered. A Hamilton population decomposition of the energy of Pt-Pt interaction underneath H and for a pure Pt surface is presented in tabular form at the bottom.

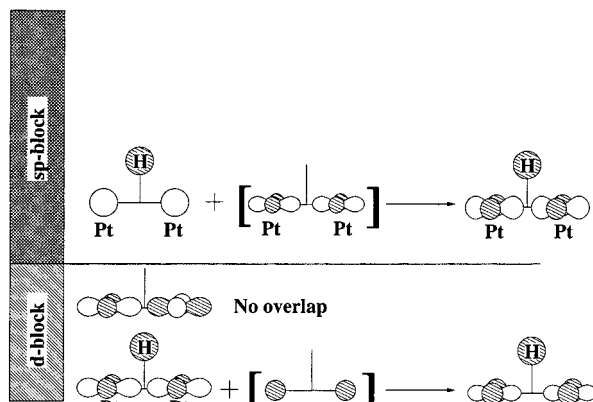


Figure 15. A schematic diagram of a second-order $s-d_{x^2-y^2}$ mixing induced by H for the Pt-Pt bond underneath H. A local viewpoint is emphasized.

bonding s-crystal orbitals into lower-lying bonding d-crystal orbitals, in such a way as to stabilize the H-Pt interactions (Figure 15). However, there is a downside for this mixing with respect to the strength of the Pt-Pt bonds: s orbitals mix out-of-phase with $d_{x^2-y^2}$ orbitals (see Figures 14 and 15). The resulting s-d Hamilton population (while still bonding) becomes destabilized by 0.43 eV compared to the pure Pt surface. A

Table 5. COHP Decomposition of Various Interactions for an fcc Chemisorbed H on Pt(111)^a

H-Pt COHP Analysis		
	H-FCC	H-Atop
s(H)-s(Pt)	-6.59 eV	-4.99 eV
s(H)-p(Pt)	-3.41 eV	-3.62 eV
s(H)-d(Pt)	-3.24 eV	-3.38 eV
Total H-Pt	-13.24 eV	-12.00 eV

Pt-Pt off-site COHP (in eV)			
H-FCC		Pure Pt slab	
Surface Pt-Pt	-1.36	Surface Pt-Pt	-1.94
	-1.92		-1.94
"Bulk" Pt-Pt	-1.83	"Bulk" Pt-Pt	-1.88

Surface Pt orbital populations

	d	s	p
Pure Pt slab	9.35	0.42	0.20
H-FCC*	9.24	0.44	0.23
H-Atop*	8.75	0.55	0.37

*Only Pt atoms connected to H are considered

^a Surface Pt-Pt bonds in the Pt₃ triangles underneath H are indicated with bold lines. The atomic orbital populations are presented as well.

similar H-induced mixing of higher-lying p-crystal orbitals into the d-crystal orbitals brings a 0.26 eV destabilization of the p-d HP value as well.

Another contribution to the weakening of the Pt-Pt bond comes from the d-d Hamilton population term (Figure 14). The origin of this effect becomes clear if the local symmetry of the surface orbitals is examined (Figure 15). The antibonding d orbitals possess a node between Pt atoms that makes their subsequent overlap with incoming H zero. The bonding crystal orbitals, on the other hand, are well-suited for strong interactions with H. Thus, those surface crystal orbitals which are bonding with respect to the Pt-Pt bond underneath H are pushed up by mixing with H. Since they are lower in energy than corresponding antibonding orbitals, a smaller number of these states reach the Fermi level and depopulate, compared with atop H (compare d-orbital populations for atop and bridge cases in Table 4). But even the smaller depopulation of these d-d bonding orbitals brings about 0.24 eV destabilization of d-d HP. We conclude, therefore, that the second-order mixing of s,p states into d states through the adsorbed H is the main factor responsible for the 0.69 eV diminution of the Pt-Pt Hamilton population, followed by the 0.24 eV diminution due to the d-d bonding state depopulation.

The total energy for H on the fcc site is approximately the same as that for the bridge site, i.e., it is slightly destabilized compared to the atop adsorption. One may observe in Table 5 essentially the same features of various off-site HP values as for the bridge case. Notice that the H-Pt COHP values given in Tables 3-5 represent only a small fraction of the extended Hückel total energy, i.e., the contribution of other off-site and on-site COHP terms must be considered as well. For instance, the H-Pt (surface) Hamilton population is much stronger for fcc H than for atop H, but that is more than compensated by the weakening of Pt-Pt bonds in Pt₃ triangles underneath H. The same factors are in play here as for the bridge case, i.e.,

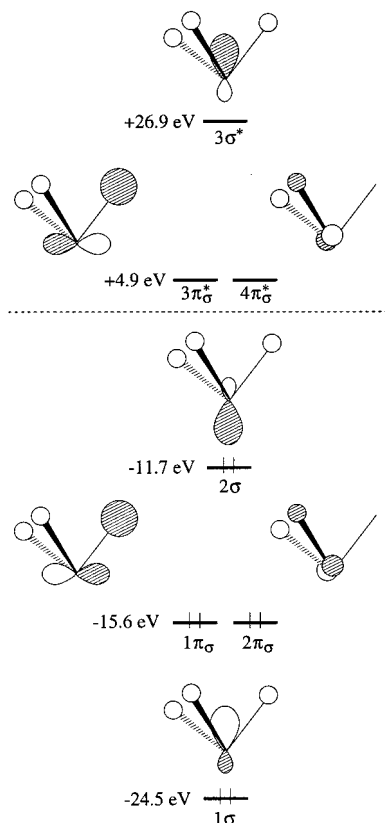


Figure 16. CH₃ fragment molecular orbitals and their respective energies as calculated with the extended Hückel method.

symmetric bands interact stronger and become partially depopulated, leading to the destabilization of the d–d Hamiltonian population. More importantly, the same mechanism of second-order s–d and p–d mixing of surface orbitals induced by adsorbed H results in a significant destabilization of the surface Pt–Pt bonds.

In summary, an H atom interacts more strongly with the Pt surface in the higher symmetry bridge and fcc sites than in the atop site, but the specific symmetry of surface orbitals at the bridge and fcc sites causes unfavorable mixing of Pt surface states. The Pt–Pt bonding d–d states become partially depopulated; in addition significant destabilization develops for s–d and p–d interactions due to second-order mixing through adsorbed H. In other words, the Pt–H bond strengthening on the bridge and fcc sites is accompanied by weakening of the corresponding surface Pt–Pt bonds. As a result, all three sites exhibit essentially the same H chemisorption binding energies within the accuracy of both Planewave DFT and extended Hückel methods. Given the small size of the conformational space, we conclude that the potential energy surface for H on Pt(111) is rather flat.

Methyl and ethyl groups, in contrast, display very strong preference for the atop site, as indicated by our DFT results. In the following analysis we try to understand the molecular orbital interactions behind the CH₃ chemisorption which so clearly set it apart from H.

3.6. CH₃ on the Atop Site. Having in mind organic analogues, one is naturally inclined to think that the CH₃ group should have bonding patterns similar to H. There is an orbital rationale behind this as well: the frontier CH₃ 2σ lone pair in Figure 16 has a similar energy and somewhat similar (if more directional) shape as the H 1s orbital. Of course, one makes here the implicit assumption that the other CH₃ Fragment

Table 6. COHP Decomposition of Various Interactions for an Atop Chemisorbed CH₃ on Pt(111)^a

CH ₃ 2σ-Pt* orb. COHP		CH ₃ FMO - Pt* COHP	
s(Pt)	-3.53 eV	1σ	+0.98 eV
p(Pt)	-2.28 eV	1π	+0.27 eV
d(Pt)	-3.37 eV	2π	+0.27 eV
	-9.18 eV	2σ	-9.19 eV
		3π*	-0.10 eV
		4π*	-0.10 eV
		3σ*	-0.55 eV
COHP Pt-H	+0.48 eV (repulsive)		-8.42 eV

Pt-Pt off-site COHP (in eV)			
CH ₃ -Atop		Pure Pt slab	
Surface Pt-Pt	-2.04	Surface Pt-Pt	-1.94
	-1.88		-1.94
"Bulk" Pt-Pt	-1.82	"Bulk" Pt-Pt	-1.88

Surface Pt orbital populations

	d	s	p
Pure Pt slab	9.35	0.42	0.20
CH ₃ -Atop*	8.84	0.53	0.32

*Only Pt atoms connected to C are considered

^a Surface Pt–Pt bonds originating from Pt underneath H are indicated with bold lines. The atomic orbital populations are presented as well.

Molecular Orbitals (FMO) do not play a significant role in the CH₃ reactivity (see Figure 16). In the following discussion we examine in detail each of the abovementioned assumptions. As we will see, CH₃ is similar to H in some adsorption sites, and different on others.

As we have mentioned earlier, the COHP analysis may be carried out in the orbital, atomic, and fragment basis. In the H chemisorption analysis we have used so far only the two former ones; the latter comes in particularly handy for studying the contributions of various CH₃ FMO's into the total Hamiltonian population. A selected set of the Hamiltonian population values for CH₃ adsorbed on the atop site is given in Table 6. The comparison of Pt s-, p-, and d-orbital contributions into the total CH₃–Pt HP with the corresponding values for adsorbed H indicates that the former interactions are somewhat weaker (Tables 3 and 6). This conclusion is further supported by the lesser depopulation of the Pt d states, i.e., fewer states are pushed over the Fermi level.

The CH₃ FMO by FMO decomposition of the CH₃–Pt HP suggests that the abovementioned hypothesis of the CH₃ 2σ "radical lobe" FMO being by far the most important one is essentially correct. Another interesting feature seen in Table 6 is the antibonding contributions from CH₃ FMO's 1σ, 1π_σ, and 2π_σ, and correspondingly bonding contributions from higher-lying FMO's 3π_σ*, 4π_σ*, and 3σ*. The former FMO's are filled bonding orbitals and their subsequent interactions with the filled Pt surface states may be described qualitatively as a four-electron two-orbital repulsion. On the contrary, the CH₃ antibonding FMO's are empty, thus they serve as acceptor orbitals for the filled Pt surface states (i.e. metal to adsorbate back-donation). The effects are not large for both overlap and energy separation reasons.

We again observe selective strengthening of Pt–Pt bonds originating from Pt underneath CH₃ (Table 6), as found also

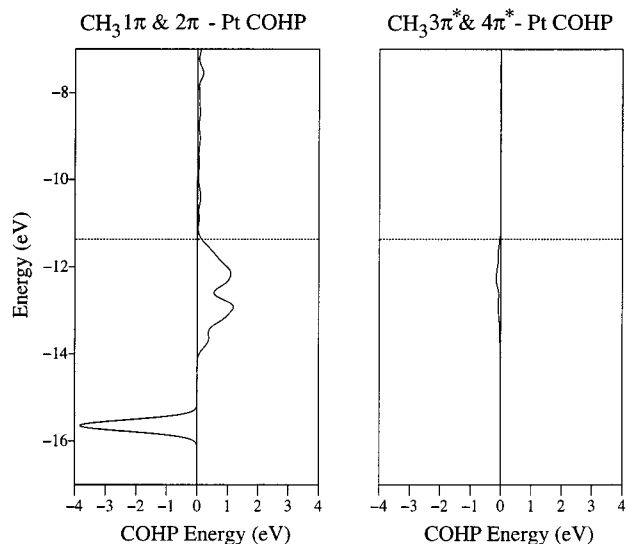


Figure 17. The COHP curves (solid lines) and their respective integrations (dotted lines) for CH_3 π_σ -FMO's with the Pt directly underneath H.

for the atop H on Pt(111). Comparison of the changes in the surface Pt d–d COHP curves due to CH_3 adsorption with the corresponding H curves suggests that the strengthening mechanism is the same; the top antibonding portion of the d block interacts much more strongly with CH_3 FMO 2σ and is partially depopulated. Furthermore, the horizontal polarization of the Pt surface bonds may be traced to the same origins as elaborated earlier in the H case. Therefore, in the atop site, the CH_3 FMO 2σ and H $1s$ orbital interactions with the Pt surface are rather similar (although the former interaction is somewhat weaker).

In addition to C–Pt bonding, the methyl H–Pt contacts are close enough to be important as well. We have calculated a +0.48 eV off-site HP value between each H and the Pt atom under CH_3 . To understand in more detail the orbital nature of this repulsion, we have plotted in Figure 17 the CH_3 π_σ -Pt COHP curves. It is the CH_3 π_σ fragment MO's which have substantial H character. First, we observe that the filled bonding π_σ FMO's interact much stronger with the surface than the corresponding empty π_σ^* FMO's. Second, the interaction of filled π_σ orbitals with the filled Pt states may be described as a four-orbital two-electron repulsion, with bonding and antibonding combinations both occupied.

In summary, the perturbational description of the chemisorption mechanism depicted for H in Figure 11 continues to be a valid model for the adsorbed CH_3 group as well. The important difference comes from the existence of not one but several CH_3 fragment orbitals, although the CH_3 lone pair orbital plays by far the most important role. The latter interacts strongest with the top portion of the d block, for the same reasons (having to do with the initial s–d hybridization of Pt surface states) as were previously found for the atop chemisorbed H. The filled CH_3 π_σ FMO's are engaged in repulsive interactions with the filled Pt surface states, which explains the destabilizing character of the H–Pt Hamilton populations.

3.7. CH_3 on the Bridge and fcc Sites. The binding energy for bridge CH_3 , as calculated by the Planewave DFT method, is 0.61 eV higher than that for atop CH_3 (Figure 2). Extended Hückel results reproduce the same tendency, yet exaggerating it a little: the bridge position is destabilized by 0.80 eV. Recall that the H adsorption was equally preferred in both sites, stronger Pt–H bonding on the bridge site being compensated by weakening of the surface Pt–Pt bond. We have also demon-

Table 7. COHP Decomposition of Various Interactions for a Bridge Chemisorbed CH_3 on Pt(111)^a

$\text{CH}_3 2\sigma$ -Pt* orb. COHP		CH_3 FMO - Pt* COHP	
s(Pt)	-3.44 eV	1σ	+1.48 eV
p(Pt)	-1.99 eV	1π	+0.30 eV
d(Pt)	-2.73 eV	2π	-1.35 eV
	-8.16 eV	2σ	-8.16 eV
		$3\pi^*$	-0.29 eV
		$4\pi^*$	-0.07 eV
		$3\sigma^*$	-0.45 eV
			-8.54 eV

Pt-Pt off-site COHP (in eV)	
CH_3 -Bridge	Pure Pt slab
Surface Pt-Pt — -1.54	Surface Pt-Pt — -1.94
Surface Pt-Pt — -1.86	Surface Pt-Pt — -1.94
"Bulk" Pt-Pt -1.82	"Bulk" Pt-Pt -1.88

Surface Pt orbital populations			
	d	s	p
Pure Pt slab	9.35	0.42	0.20
CH_3 -Bridge [†]	9.14	0.45	0.26

[†]Only Pt atoms connected to C are considered

^a Surface Pt–Pt bonds originating from Pt underneath H are indicated with bold lines. The atomic orbital populations are presented as well.

strated above that the methyl group in the atop position binds much in the same way as hydrogen. Thus, the difference in binding site preference must be coming from special features of CH_3 adsorption in the bridge position.

A selection of bridge- CH_3 Hamilton population values are collected in Table 7. Since the H $1s$ orbital interacts more strongly with the Pt surface in the bridge site, and the CH_3 2σ FMO is isolobal to the H $1s$ orbital, one might reasonably expect for 2σ -Pt HP to be more bonding on the bridge site. However, the opposite happens. The total 2σ -Pt Hamilton population of -9.19 eV on the atop site drops by 1.03 eV to -8.16 eV on the bridge site (Tables 7 and 6). If the 2σ -Pt HP is partitioned into Pt s, p, and d contributions, then one observes a destabilization of all of these compared to the atop case. The latter two contributions are destabilized the most.

In addition to CH_3 2σ -Pt interactions being less bonding on the bridge site, the Pt–Pt bond underneath CH_3 weakens as well, as was also found for bridge chemisorbed H (although to a smaller degree). The same mechanism is operative for the bridge Pt–Pt bond destabilization: the symmetric bonding d bands interact strongest, being pushed up and becoming partially depopulated; in addition, second-order CH_3 induced mixing of higher-lying s,p states into the d states significantly weakens the Pt–Pt bond. Thus, neglecting for the moment other CH_3 FMO's, the reason for less favorable bonding at the bridge site is that 2σ -Pt and Pt–Pt interactions are simultaneously destabilized.

The next question we face is the following: why does the chemisorbed H $1s$ orbital have more favorable interactions with Pt atoms in the bridge site than the chemisorbed CH_3 2σ lone pair? To find an answer, we have computed the corresponding

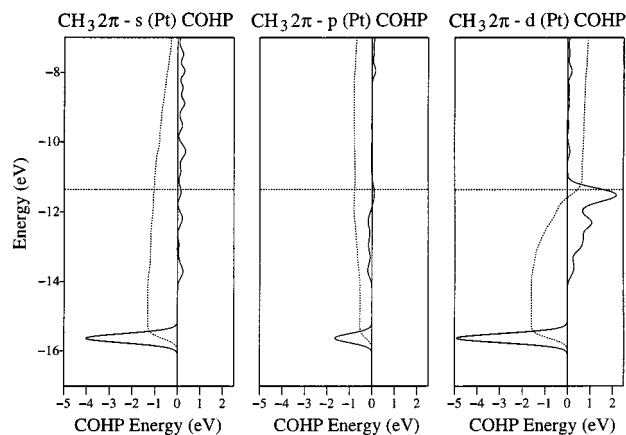


Figure 18. The COHP curves (solid lines) and their respective integrations (dotted lines) for CH_3 $2\pi_\sigma$ -s(Pt), $2\pi_\sigma$ -p(Pt), and $2\pi_\sigma$ -d(Pt) interactions for the CH_3 on the bridge site.

overlap values between various Pt s, p, and d atomic orbitals and H 1s and CH_3 2σ in the atop and the bridge sites (not shown here). Indeed, we have found that the bridge/atop overlap ratio is significantly higher for H 1s than for CH_3 2σ . This overlap difference may be further explained by the approximate sp^3 hybridization of CH_3 2σ , its p component having poor overlap with the Pt atomic orbitals on the bridge site.

In the atop site, on the contrary, the p-orbital lobe points exactly at the Pt s, p_z and d_{z^2} orbitals. We have here a strong indication that for purely overlap reasons a hydrocarbon lone pair must be pointing directly at Pt for that interaction to be the strongest.

While the CH_3 2σ FMO is dominant, we should examine other CH_3 FMO's as well. If these interactions are considered, then the total bridge CH_3 -Pt Hamilton population is more favorable by -0.16 eV than in the atop position. This effect is largely attributed to a quite stabilizing CH_3 $2\pi_\sigma$ -Pt HP value of -1.35 eV, compared with repulsive $+0.54$ eV on the atop site. Notice that FMO $1\pi_\sigma$ of the previously degenerate CH_3 π_σ set is largely unaffected; the degeneracy of the CH_3 π_σ -type MO interactions is broken by the specific position of the Pt-Pt bond underneath.

To probe in more detail for the nature of the $2\pi_\sigma$ -Pt interactions, we have projected out various Pt s, p, and d contributions (Figure 18). The $2\pi_\sigma$ -d(Pt) COHP curves are characteristic of four-electron two-orbital repulsion between filled orbitals with bonding and antibonding regions both filled. The $2\pi_\sigma$ -s(Pt) and $2\pi_\sigma$ -p(Pt) projections, however, more than reverse the effect of this repulsion. Therefore, the empty Pt s and p bands serve as acceptor orbitals for the $2\pi_\sigma$ electron density. This is consistent with a diminution the $2\pi_\sigma$ FMO population from 1.99 for atop CH_3 to 1.92 for bridge CH_3 . At the bridge site a number of Pt surface s and p orbitals match the local π symmetry of the $2\pi_\sigma$ FMO, while in the atop position these overlaps are negligible. For instance, the Pt s orbital and the CH_3 $2\pi_\sigma$ FMO belong to different local symmetry groups for atop chemisorbed CH_3 (weaker next-nearest-neighbor overlaps are still expected).

The stabilizing $2\pi_\sigma$ -Pt surface interaction leads to a bonding H-Pt HP value of -0.44 eV for the methyl H pointing at the neighboring Pt. On the contrary, the H-Pt Hamilton populations for atop CH_3 were found to be repulsive ($+0.48$ eV). However, the depopulation of the bonding CH_3 $2\pi_\sigma$ FMO results in substantial weakening of the C-H bond HP, by 1.10 eV as compared to the C-H HP for the atop CH_3 . These conclusions are consistent with the Planewave DFT optimized bridge CH_3

geometries: one of the C-H bonds is found to be aligned parallel to the bridge Pt-Pt bond and it is slightly elongated to 1.12 Å. While this elongation seems small it is significant, nevertheless, given the rather steep potential energy surface for the C-H bond stretching. The H-Pt distance of 2.10 Å is actually shorter than the corresponding C-Pt bond lengths (2.33 Å). Thus we suggest that significant agostic interaction exists between the bridge-parallel C-H bond and the neighboring Pt atom (Figure 2).

Weakening of C-H bonds would manifest itself in softening of C-H stretching vibrational modes, as is indeed observed for CH_3 on Ni(111) and Cu(111)^{18-20,49} On these surfaces the CH_3 group is thought to occupy a 3-fold site. This softening is generally attributed to the back-donation of metal d electrons into the C-H antibonding orbitals.¹⁹ Our COHP analysis strongly suggests that this is not the case; we find that the antibonding C-H orbitals play a very minor role, and the agostic interactions may be described qualitatively as a donation of C-H bonding electron density into metal empty s and p bands (see Table 7 and Figure 18).

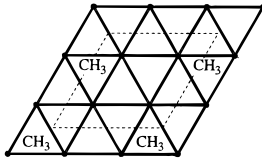
Demuth and co-workers, followed by other authors, observed significant softening of cyclohexane C-H vibrations on transition metal surfaces, including Pt(111) and Ni(111).^{61,62} Sheppard and De La Cruz arranged transition metals with respect to their ability to increasingly soften C-H vibrations as Cu, Ni, Pd, Pt, and Ru.⁴⁹ The transformation of cyclohexane to benzene (C-H bond activation) was observed on Pt(111) but not on Ni(111), which confirms this trend.⁶¹ On the former surface, three initially soft cyclohexane C-H bonds, which interact strongest with the Pt surface, dissociate when heated above 200 K, as found by Land, Erley, and Ibach.⁶² From all the experimental evidence presented above, one would expect for 2- or 3-fold adsorbed CH_3 on Pt(111) to exhibit even more C-H mode softening than on Ni(111). The absence of such softening for both methyl and ethyl groups on Pt(111) quite unambiguously points to the atop chemisorption of these species (a similar conclusion may be drawn for CH_3 on Ru(0001)).⁴⁹

As for the CH_3 adsorption at the fcc site, it parallels the bridge CH_3 case. The CH_3 2σ -Pt Hamilton population of -8.54 eV is again less bonding than that for the atop case (-9.19 eV). Coupled with significant weakening of Pt-Pt bonds in the Pt_3 triangles underneath CH_3 , this renders the fcc site less attractive compared with the atop site (Table 8). According to the extended Hückel calculated total energies, the fcc site appears to be slightly less stable than the bridge site. Because of the pseudo-3-fold symmetry on the fcc site, the originally degenerate CH_3 $1\pi_\sigma$ and $2\pi_\sigma$ FMO's continue to be nearly degenerate. Their combined interaction with the Pt s and p orbitals is somewhat stronger than at the bridge site (Table 8). However, the H-Pt HP value is -0.05 eV, as there are three shared H-Pt interactions, as opposed to one for the bridge case (the other two H-Pt HP's for bridge CH_3 are repulsive at $+0.16$ eV).

We conclude from the preceding analysis that the CH_3 sp^3 lone pair has much better overlap with the surface crystal orbitals if it is pointing directly toward Pt atoms. Consequently, its interactions with the surface are weaker on the bridge and fcc sites, compounded by weakening of surface Pt-Pt bonds due to the symmetry and s,p-d mixing reasons outlined already for the H adsorption. For bridge CH_3 , the empty Pt s and p states serve as acceptor orbitals for the filled bonding CH_3 $2\pi_\sigma$ FMO, which in turn weakens the corresponding C-H bond. Agostic

(61) Demuth, J. E.; Ibach, H.; Lebwald, S. *Phys. Rev. Lett.* **1978**, *40*, 1044.

(62) Land, D. P.; Erley, W.; Ibach, H. *Surf. Sci.* **1993**, *289*, 237.

Table 8. COHP Decomposition of Various Interactions for a FCC Chemisorbed CH₃ on Pt(111)^a


CH ₃ 2σ-Pt*orb. COHP	CH ₃ FMO - Pt*COHP
s(Pt) -3.84 eV	1σ +2.05 eV
p(Pt) -2.03 eV	1π -0.78 eV
d(Pt) -2.67 eV	2π -0.78 eV
-8.54 eV	2σ -8.54 eV
	3π* -0.20 eV
	4π* -0.20 eV
	3σ* -0.45 eV
	-8.90 eV

Pt-Pt off-site COHP (in eV)			
CH ₃ -FCC		Pure Pt slab	
Surface Pt-Pt	-1.53	Surface Pt-Pt	-1.94
	-1.90		-1.94
"Bulk" Pt-Pt	-1.82	"Bulk" Pt-Pt	-1.88

Surface Pt orbital populations			
	d	s	p
Pure Pt slab	9.35	0.42	0.20
CH ₃ -FCC*	9.26	0.43	0.24

*Only Pt atoms connected to C are considered

^a Surface Pt–Pt bonds originating from Pt underneath H are indicated with bold lines. The atomic orbital populations are presented as well.

interactions in bridging and 3-fold sites are found, driven by interactions between the nearly degenerate set of CH₃ π_o's and the Pt surface states. This picture is consistent with the experimentally observed cyclohexane C–H stretching mode softening and eventual dissociation on the Pt(111) surface.

3.8. Why Is Ni Different? As mentioned in the beginning of our discussion, the CH₃ group preferentially binds in a 3-fold site on Ni(111), in contradiction with the tetravalency rule. A comparative Ultraviolet Photoemission Spectroscopy (UPS) study by Demuth of the H chemisorption on Ni, Pd, and Pt provides a significant clue for our understanding of this difference: the author observed a much smaller participation of Ni d bands in bonding with H as compared with Ni s,p bands.²⁸ The role of d orbitals was found to be much more important for H chemisorbed on Pd(111) and Pt(111).²⁸ Demuth attributed the different behavior of Ni compared to Pd and Pt to the contracted nature of 3d orbitals, which are radially nodeless. For instance, Hammer and Nørskov suggested a 3-fold reduction in the s (H)–d (metal) coupling matrix element for Ni compared with Pt.⁶⁰

In a hypothetical thought experiment, let us assume for a moment the complete absence of Ni 3d interactions with H or CH₃. As we have established in our earlier analysis, the metal s orbitals are engaged in stronger interactions with the adsorbate in the 3-fold positions than on the atop position (for H compare Tables 3 and 5, for CH₃ Tables 6 and 8). Were there no d-orbital participation, the metal–metal bonds would be less weakened in the high-symmetry sites, since no unfavorable s–d mixing and depopulation of bonding d–d states would occur. Thus, if s bands would strongly dominate bonding, the 3-fold site might be expected to be preferred both for H and CH₃, with accompanying agostic interactions for the latter species.

To examine these conclusions, the overlaps between Pt d orbitals and CH₃ orbitals were set to zero in a numerical experiment. Indeed, our extended Hückel calculations indicate that the 1.01 eV preference for on-top CH₃ compared with fcc CH₃ reduces to only 0.19 eV if CH₃ does not interact with the Pt d orbitals. Although the on-top adsorption is still preferred, the tendency is clearly demonstrated. The experimental results strongly suggest that the CH₃ group occupies a 3-fold position on Ni(111) and Cu(111), and an atop position on Pt(111) and Ru (0001).⁴⁹

Of course, Ni d bands *do* interact with the adsorbates, however, to a smaller degree than for Pd and Pt. This makes their respective (111) surfaces quite dissimilar.⁶⁰ The reasoning provided above is still speculative at this point, although based on the extensive experience from our calculations on Pt(111) as well as on the earlier experimental suggestions. These conclusions are also supported by recent DFT slab calculations for H and CH₃ on the Pd(111) surface and the Ni(111) surface.^{63–66} For example, Paul and Sautet found essentially no difference in adsorption energies between various adsorption sites for CH₃ on Pd(111).⁶⁵ As for CH₃ on Ni(111), Hu and Michaelides found a relatively small ≈0.2 eV preference for the 3-fold site adsorption compared with the atop adsorption.⁶⁶ Thus, when going from Pt to Pd and then to Ni, the methyl group site preference shifts gradually from an atop to higher-coordinated positions.

The theory of H and CH₃ chemisorption that we have constructed for Pt(111) may not be simply transferred to 3d transition metals. For the latter the higher symmetry sites are expected to be favored; thus the tetravalency principle definitely does not apply to them. As all transition metals are characterized by their own peculiarities, extreme care has to be exercised when proposing general principles of chemisorptive bonding.

4. Conclusions

Our Planewave DFT calculations for methyl and ethyl groups are consistent with the previously proposed tetravalency principle of hydrocarbon chemisorption, i.e., these groups bind strongest on the atop site. Hydrogen, however, does *not* show a clear adsorption site preference. Given the isolobal correspondence between H and CH₃ (C₂H₅), such behavior needed to be explained. We have also endeavored to build a comprehensive molecular orbital theory of H and small hydrocarbon chemisorption on Pt(111) which rationalizes and expands the original tetravalency rule. A newly developed theoretical method, the Crystal Orbital Hamilton Population formalism, has served as a primary tool for our analysis.

It turns out that the initial s–d and p–d hybridization of Pt bands in a pure Pt slab and the specific symmetry properties of surface orbitals at various sites are the most important factors determining the reactivity of the Pt surface. For instance, for the H atom adsorbed in the atop position, only the top portion of the d_{z²} band is so hybridized as to overlap strongly with the H 1s orbital. Since the latter is found lower in energy, it pushes up the Pt d–d antibonding states, some of which reach the Fermi level and depopulate. Thus, Pt–Pt bonds originating from Pt underneath H are strengthened, behaving very differently from

(63) (a) Paul, J. F.; Sautet, P. *Phys. Rev. B* **1996**, *53*, 8015. (b) Paul, J. F.; Sautet, P. *Surf. Sci.* **1996**, *356*, L403.

(64) Watwe, R. M.; Bengaard, H. S.; Rostrup-Nielsen, J. R.; Dumesic, J. A.; Nørskov, J. K. *J. Catal.* **2000**, *189*, 16.

(65) Paul, J. F.; Sautet, P. *J. Phys. Chem. B* **1998**, *102*, 1578.

(66) Hu, P.; Michaelides, A. *Surf. Sci.* **1999**, *437*, 362.

(67) Summerville, R. H.; Hoffmann, R. *J. Am. Chem. Soc.* **1976**, *98*, 7240.

the remaining surface bonds. We have shown a detailed molecular orbital mechanism for such a lateral polarization of the surface states. Although the Pt(111) surface is rigid in nature, one could imagine that this mechanism is important for other surfaces (and other metals), providing potentially some understanding of adsorbate-induced surface reconstruction.

A H atom adsorbed at bridge and fcc sites on Pt(111) exhibits stronger H–Pt bonds (gauged by the corresponding Hamilton populations) than on the atop site. We have attributed this change mainly to the better interactions with the Pt *s* orbitals. The overall stability is slightly diminished, however; the Pt–Pt bonds underneath H get significantly weakened, offsetting the stabilization of H–Pt contacts. We have been able to trace the weakening of surface Pt–Pt bonds to unfavorable H-induced second-order mixing of Pt *s,p* bands into the *d* block. In addition, the partial depopulation of strongly interacting *d*–*d* symmetric bonding bands also leads to Pt–Pt bond weakening.

Methyl group chemisorption on the Pt(111) surface is shown to have much similarity with H adsorption. For example, in the atop site, the CH₃ 2*σ* lone pair interacts much the same way with the antibonding portion of the *d* block, partially depopulating it. Thus, selective strengthening of Pt–Pt bonds originating from Pt under CH₃ is observed computationally as for the H case. The same mechanism of Pt surface polarization is found for adsorbed CH₃ as well. The CH₃ filled 1*π_σ* and 2*π_σ* FMO's engage in four-electron two-orbital repulsion with filled Pt *d* states, thus rendering methyl H–Pt interactions antibonding.

The greatest differences between chemisorbed CH₃ and H are found for the bridge and fcc sites. The CH₃ 2*σ* lone pair, sp³ hybridized, does not overlap as well with the surface states when pointing into the center of a Pt–Pt bond or a Pt₃ triangle. In addition, the same mechanism of CH₃-induced weakening of Pt–Pt bonds underneath CH₃ (as for H on bridge and fcc sites) operates. Simultaneous weakening of CH₃ 2*σ*–Pt bonding and Pt–Pt bonding makes the higher symmetry sites very unfavorable for the CH₃ chemisorption. A similar trend is to be expected for the C₂H₅ binding site preference, as evidenced by our Planewave DFT calculations.

While CH₃–Pt bonding in high-symmetry sites is unfavorable (relative to the atop site), it has an interesting feature: it is strengthened by agostic interactions between C–H bonds and the Pt surface. For the bridge site, for example, the CH₃ filled 2*π_σ* FMO donates its electron density to Pt empty *s* and *p* states, rendering the methyl H to neighboring Pt contacts quite bonding. As expected, weakening of the corresponding C–H bond occurs as well, in agreement with the Planewave DFT optimized elongated C–H bond distance. Given the higher local symmetry of the fcc site, all three C–H bonds are engaged in agostic interactions with the Pt surface. Our suggestions are in agreement with the C–H mode softening for cyclohexane on Pt(111) as well as for 3-fold bound CH₃ on Cu(111) and Ni(111).

In this work, we have constructed a comprehensive molecular orbital theory of H and small hydrocarbon chemisorption, perturbational in nature. This has helped us to understand the molecular orbital reasons behind the different site preferences of H and CH₃ on Pt(111). We have also speculated, citing earlier UPS suggestions, that for 3*d* transition metals the *s,p* interactions with the adsorbate dominate, which in turn explains the CH₃ preference for the 3-fold site on Ni(111) and Cu(111) and for the atop site on Pt(111) and Ru (0001).

In the forthcoming study, we will report the Planewave DFT optimized geometries and binding energies for a number of other hydrocarbons, including ethylene and ethylidyne, which are suspected to be the important intermediate species in the hydrogenation process.

Acknowledgment. We would like to thank Wingfield Glassey for helpful discussions. Our work in the field was stimulated by a correspondence and the ideas of Gabor Somorjai. We gratefully acknowledge the National Science Foundation for its generous support of this work by Research Grant CHE-9970089 and the Cornell Theory Center for computer time. We thank the members of CAMP at the Technical University of Denmark for help with the initial part of this project.

JA993483J